Since January 2020 Elsevier has created a COVID-19 resource centre with free information in English and Mandarin on the novel coronavirus COVID-19. The COVID-19 resource centre is hosted on Elsevier Connect, the company's public news and information website.

Microbial Risk Analysis 16 (2020) 100140

Contents lists available at ScienceDirect

Microbial Risk Analysis

journal homepage: www.elsevier.com/locate/mran

Thermodynamic equilibrium dose-response models for MERS-CoV infection reveal a potential protective role of human lung mucus but not for SARS-CoV-2

Paul Gale*

Independent Scientist, 15 Weare Close, Portland, Dorset, DT5 1JP, UK.

ARTICLE INFO

Keywords:
SARS-CoV-2
Infection
Dose-response
Mucin
Risk

ABSTRACT

Severe acute respiratory syndrome coronavirus 2 (SARS-CoV-2) and Middle East respiratory syndrome coronavirus (MERS-CoV) infect the human respiratory tract. A prototype thermodynamic equilibrium model is presented here for the probability of the virions getting through the mucus barrier and infecting epithelial cells based on the binding affinity (K_{mucin}) of the virions to mucin molecules in the mucus and parameters for binding and infection of the epithelial cell. Both MERS-CoV and SARS-CoV-2 bind strongly to their cellular receptors, DDP4 and ACE2, respectively, and infect very efficiently both bronchus and lung ex vivo cell cultures which are not protected by a mucus barrier. According to the model, mucin binding could reduce the infectivity for MERS-CoV compared to SARS-CoV-2 by at least 100-fold depending on the magnitude of K_{mucin}. Specifically K_{mucin} values up to 10^6 M^{-1} have little protective effect and thus the mucus barrier would not remove SARS-CoV-2 which does not bind to sialic acids (SA) and hence would have a very low K_{mucin}. Depending on the viability of individual virions, the ID_{50} for SARS-CoV-2 is estimated to be ~500 virions (viral RNA genomic copies) representing 1 to 2 pfu. In contrast MERS-CoV binds both SA and human mucin and a K_{mucin} of 5×10^9 M^{-1} as reported for lectins would mop up 99.83% of the virus according to the model with the ID_{50} for MERS-CoV estimated to be ~295,000 virions (viral RNA genomic copies) representing 819 pfu. This could in part explain why MERS-CoV is poorly transmitted from human to human compared to SARS-CoV-2. Some coronaviruses use an esterase to escape the mucin, although MERS-CoV does not. Instead, it is shown here that "clustering" of virions into single aerosol particles as recently reported for rotavirus in extracellular vesicles could provide a co-operative mechanism whereby MERS-CoV could theoretically overcome the mucin barrier locally and a small proportion of 10 μm diameter aerosol particles could contain ~70 virions based on reported maximum levels in saliva. Although recent evidence suggests SARS-CoV-2 initiates infection in the nasal epithelium, the thermodynamic equilibrium models presented here could complement published approaches for modelling the physical entry of pathogens to the lung based on the fate and transport of the pathogen particles (as for anthrax spores) to develop a dose-response model for aerosol exposure to respiratory viruses. This would enable the infectivity through aerosols to be defined based on molecular parameters as well as physical parameters. The role of the spike proteins of MERS-CoV and SARS-CoV-2 binding to SA and heparan sulphate, respectively, may be to aid non-specific attachment to the host cell. It is proposed that a high K_{mucin} is the cost for subsequent binding of MERS-CoV to SAs on the cell surface to partially overcome the unfavourable entropy of immobilisation as the virus adopts the correct orientation for spike protein interactions with its protein cellular receptor DPP4.

1. Introduction

Severe acute respiratory syndrome coronavirus 2 (SARS-CoV-2) emerged in December 2019, causing a respiratory disease (coronavirus disease 2019, COVID-19) of varying severity in Wuhan, China, subsequently leading to a pandemic (Hui et al 2020). By 8 Aug 2020 there had been some 19.4 million cases of SARS-CoV-2 worldwide with 721,906 deaths globally (Anon 2020). Like SARS-CoV-2 other beta coronaviruses (CoVs) such as severe acute respiratory syndrome virus (SARS-CoV) and Middle East respiratory syndrome coronavirus (MERS-CoV) also infect the human respiratory tract and causes severe zoonotic respiratory disease. MERS-CoV is transmitted sporadically to humans

* Corresponding Author.
E-mail address: paul@galleryofbirds.com.

https://doi.org/10.1016/j.mran.2020.100140
Received 7 June 2020; Received in revised form 9 August 2020; Accepted 11 September 2020
Available online 19 September 2020

from its dromedary camel (*Camelus dromedarius*) reservoir, causing severe respiratory disease with ~35% fatality rate (Li et al. 2017). A major difference is that both SARS-CoV and SARS-CoV-2 are readily transmitted between humans by close contact, while MERS-CoV is not (Rabaan et al. 2020). Person-to-person community transmission of SARS-CoV-2 is highly efficient while MERS-CoV is transmitted occasionally by human-to-human contact (Killerby et al.2020) through infectious aerosolized particles often in hospital settings (Adhikawi et al. 2019). Thus, humans are considered transient or terminal hosts for MERS-CoV, with no evidence for sustained human-to-human community transmission. In naturally infected camels, MERS-CoV RNA has been recovered most commonly from nasal swabs but also from faecal swabs, rectal swabs, and lung tissue (Killerby et al. 2020). Levels of MERS-CoV RNA and SARS-CoV-2 RNA copies per cm^3 of sputum or tracheal aspirate in infected humans are similar with median MERS-CoV levels of $10^{5.5}$ copies (mild group) to $10^{7.2}$ copies (severe group) (Oh et al. 2016) and median SARS-CoV-2 levels of $10^{5.9}$ to $10^{6.7}$ copies (Pan et al. 2020;To et al. 2020). This suggests these two viruses differ fundamentally in their infectiousness to humans. All three viruses infect bronchus and lung cells with high efficiency and indeed MERS-CoV seems to be the most efficient. Specifically in bronchus cell cultures, MERS-CoV replication competence is similar to that for SARS-CoV-2 and higher than SARS-CoV while in lung cell cultures, MERS-CoV-2 replication is higher than SARS-CoV and SARS-CoV-2 (Hui et al. 2020). While SARS-CoV-2 spike protein may not bind to sialic acid (SA) glycans (Hao et al. 2020) and hence to human mucins, that MERS-CoV spike protein does bind human mucin is well-documented (Li et al. 2017). Since both SARS-CoV-2 and MERS-CoV spike proteins bind strongly to their respective cellular receptors, it may be other factors such as differences in mucin binding affinity that affect infectivity. This is addressed here.

Previously a thermodynamic mechanistic approach was developed to use molecular biology data measured using biochemical methods to calibrate a dose-response model for a virus infecting the human intestine (Gale 2018). Here that model is developed for respiratory viruses such as MERS-CoV and SARS-CoV-2 by focusing on the removal of virus by mucus in the lung through entrapment (Zanin et al. 2016). The objective of this paper is to demonstrate a method to calibrate part of a dose-response model for respiratory viruses such as MERS-CoV and SARS-CoV-2 using available thermodynamic data for the key molecular interactions between the human host and viral factors during each stage of the infection process. The physical barriers and transport of the virions in the airways also have to be included in the model as for inhaled anthrax (Weir and Haas 2011) depending on where in the respiratory system the virus initiates infection, which may be in the nasal epithelium in the case of SARS-CoV-2 (Hou et al. 2020). A key physical barrier is the mucus gel layer which consists of 97% water and 3% solids, representing polymeric mucins. In its protective role, mucus entraps microbes and particles removing them from the lungs via the co-ordinated beating of motile cilia (Ridley and Thornton 2018). The major mucins produced in the airways of the human lung are the secreted polymeric mucins MUC5AC and MUC5B (Ridley and Thornton 2018) and present a barrier to respiratory viruses including influenza A virus (IAV) and adenovirus (De Graaf and Fouchier, 2014; Zanin et al. 2016; McAuley et al. 2017; Stonebraker et al. 2004). Mucins contain SA glycans to which proteins called lectins bind with high affinity, and in this respect viral surface proteins such as IAV haemagglutinin (HA) and MERS-CoV spike protein can be considered as lectins. Lectins show great specificity in the SAs to which they bind (De Graaf and Fouchier, 2014). The spike $S1^A$ protein of MERS-CoV is particularly suited to bind human respiratory mucin but not to bovine submaxillary mucin (BSM) reflecting differences in the molecular structure of the SAs (Li et al. 2017). Similarly the mouse hepatitis coronavirus (MHV) and SARS-CoV do not bind BSM (Peng et al. 2012) and to the author's knowledge it is not known if they bind human mucin. In contrast to MERS-CoV, the spike protein of SARS-CoV-2 does not bind to SA (Hao et al. 2020) suggesting it does not bind to mucins. This may represent a fundamental difference between SARS-CoV-2 and MERS-CoV and it is suggested here that this may enhance the ability of SARS-CoV-2 to diffuse through the mucus barrier to reach the lung epithelial cells compared to MERS-CoV which, it is proposed here, becomes trapped in the mucus and removed. Indeed SARS-CoV, SARS-CoV-2 and MERS-CoV are all able to replicate well in ex-vivo cultures of both human bronchus cells and lung cells (Hui et al. 2020). Unlike in the lung in vivo, cell cultures do not have a protective mucous barrier, suggesting that once through the mucus barrier, the three viruses readily infect bronchus and lung cells. Of course, there are other differences too, and the presence of a furin-like cleavage site on the spike protein in SARS-CoV-2 facilitates the spike protein priming and might also increase the efficiency of the spread of SARS-CoV-2 compared to SARS-CoV and MERS-CoV (Rabaan et al. 2020). The fact that SARS-CoV-2 may initiate infection in the nasal epithelium would also increase its human-to-human transmission efficiency.

A dose-response model has been fitted to death data for MHV in mice and also for SARS-CoV in transgenic mice expressing human angiotensin-converting enzyme 2 (hACE2) which is the receptor for SARS-CoV (Watanabe et al. 2010). The ID_{50} (death in mice through intranasal challenge) was estimated to be 280 plaque-forming units (pfu) (95% CI = 130 to 530 pfu) with p_1, the probability of death from a single virion, being 0.00246 (Huang 2013). Dose-response models such as that for MHV and SARS-CoV in mice (Watanabe et al. 2010) assume that the individual virions in a dose act independently and therefore that the risk of infection increases linearly (at low doses at least) with exposure dose, $V_{exposure}$. This may not necessarily be the case if virions in a high dose "cooperate" through overwhelming a host defence mechanism, in this case the mucins in the mucus in the lung. It is shown here for a virus that binds mucins that dispersion of the virus in the lung mucus could greatly decrease the fraction of free virus remaining to go on to infect the cells of the lung epithelium compared to the same dose concentrated (or clustered) in a single particle. Thus it is suggested here that rare, high-virion load aerosol particles may be important for MERS-CoV to get through the mucus barrier such that the virions comprising a dispersed dose may be overwhelmed by the mucin defences while the same number of virions if "acting together" may locally overwhelm the mucin defence such that more manage to get through the mucus to the lung epithelial cells. Conceptually this "co-operative action" is analogous to a team of 10 persons forming a human triangle such that one person successfully scales a high wall while acting individually none of the 10 persons can clear the wall. In contrast to MERS-CoV, aerosol particles containing a single virion of SARS-CoV-2 would be more infectious. The actual ID_{50} in terms of number of virions and the value of p_1 depend on the virion (genomic RNA copy number) to pfu ratio. It is not suggested that all those virions comprising a pfu have to co-operate to initiate infection. Instead only a small proportion of virions are viable in terms of being able to initiate infection. It is assumed that all virions whether viable or not are able to bind SA and hence bind mucin through the spike protein in the case of MERS-CoV.

The co-operative effect is only relevant if single aerosol particles small enough to get into the bronchus i.e. <10 μm in diameter (Van Leuken et al. 2016) contain multiple virions. Otherwise the virions must be considered to be fully dispersed and acting independently. A small proportion of 10 μm diameter aerosol particles as produced in coughs from IAV-infected persons (Lindsley et al. 2012) could contain multiple SARS-CoV-2 or MERS-CoV virions. Viral RNA loads for MERS-CoV and SARS-CoV-2 in infected persons of 10^9 copies per cm^3 of sputum have been reported (Oh et al. 2016; To et al. 2020) and even up to 10^{11} copies per cm^3 saliva (Adhikari et al. 2019; Pan et al. 2020). Thus Pan et al. (2020) reported a maximum viral load of SARS-CoV-2 from 80 COVID-19 patients of 1.34×10^{11} copies per cm^3 of sputum such that a 10 μm diameter particle of volume of 5.24×10^{-7} mm^3 would contain some 70 virions. It should be emphasized these high load particles would represent only a very small proportion and most

inhaled aerosol particles would contain either zero or just one virion because the median was 7.5 × 10^5 to $10^{6.7}$ copies of SARS-CoV-2 RNA per cm^3 of sputum (Pan et al. 2020;To et al. 2020). The mean for MERS-CoV was 6.3 × 10^8 copies per cm^3 saliva (Adhikari et al 2019). However, the thermodynamic dose-response model developed here does need to be able to accommodate inhalation of both particles with a single virion and particles with a cluster of virions in the case of those respiratory viruses such as MERS-CoV that bind to human mucin. Clustering mechanisms such as the secretion in stools of ~0.5 μm diameter extracellular vesicles reported by Santiana et al. (2018) as containing ~15 rotavirus virions could result in some <1 μm diameter particles which are produced in coughs in abundance (Lindsley et al. 2012) containing high virion doses although this has not been demonstrated for coronaviruses (CoVs). Lim et al. (2016) merely say that the assembly of CoV particles is completed through budding of the CoV nucleocapsid through membranes early in the secretory pathway from the endoplasmic reticulum to the Golgi. Bhar and Jones (2019) propose an alternate role (in addition to the role of virion cell binding) for the histo-blood group antigens in norovirus infection as a means of viral aggregation. Another mechanism of aggregation is through multiple viruses binding to a bacterium as in the case of human norovirus and poliovirus attaching to commensal *Enterobacter* bacteria (Bhar and Jones 2019).

2. Methods

The abbreviations are listed in Table 1.

2.1. Basic lung model

The human lung surface area was determined as 24–69 m^2 with some studies indicating the internal lung surface area to be about 130 m^2 (Fröhlich et al. 2016). Determination of the volume of the lining fluid in the lung (LLF), also called epithelial lining fluid or airway surface liquid, is more complicated than for the gastrointestinal fluids because lung volumes are much smaller. In the literature different volumes of 12 cm^3, 20–40 cm^3, 25 cm^3, 10–30 cm^3 and 17–20 cm^3 have been indicated in different studies reviewed by Fröhlich et al. (2016). Based on the body weight-dependent data obtained in sheep (0.37 ± 0.15 cm^3/kg), a 70 kg human would possess 26 cm^3 of LLF. The total number of cells in the human lung is 230 × 10^9 of which 30% are endothelial and 24% are alveolar cells (Crapo et al 1982). Lukassen et al. (2020) investigated ACE2, transmembrane protease/serine protease (TMPRSS2) and furin expression levels in the transcriptome across cell types in lung tissue. Of 39,778 lung cells studied, only 104 expressed ACE2 and TMPRSS2 and/or furin, suggesting that only 0.26% of lung cells are susceptible to infection by SARS-CoV-2. The number of cells expressing ACE2 was 206 accounting for 0.52% of the lung cells (Lukassen et al. 2020). Therefore the total number of lung cells that can bind SARS-CoV-2, C_{total}, is estimated to be 0.52% of 230 × 10^9 = 1.2 × 10^9 cells.

2.2. Thermodynamic approach for calibrating a dose-response model for infection of the human lung by a virus

Infection of the host is defined here as the infection of one or more cells in the host such that virogenesis and viral egress successfully take place in at least one cell of the host. The progeny viruses may then go on to infect other host cells leading to disease progression, which is not considered here. The response considered here, namely initial infection, happens before the innate immune response and the acquired immune response both of which are important for stopping progression of infection in the host (Lim et al. 2016). The probability, p_{host}, of being infected by airborne exposure to a given dose of virions, $V_{expsoure}$, may be described mathematically as

Table 1
List of abbreviations

(h)ACE2	**(Human) Angiotensin-converting enzyme 2**
BSM	Bovine submaxillary mucin,
CBD	Carbohydrate binding domain on a lectin or virus spike protein
CoV	Coronavirus
Cr	Host cell receptor
C_{total}	Total number of cells in human lung that have ACE2 receptors and can bind SARS-CoV-2
$C.V_T$	Number of host cells with bound virus at temperature T
dpi	Days post infection
DPP4	dipeptidyl peptidase 4 (also called CD26), protein receptor for MERS-CoV
F_c	Fraction of virus dose bound to lung cells
F_v	Fraction of virus in lung mucus not bound to mucin, i.e. free
F_{trans}	Fraction of the challenge dose, $V_{exposure}$, that is transported through the nasal airways to reach the mucus in the lung-lining fluid
GP	Viral (glyco)protein on virus surface that binds to Cr
HA	Haemagglutinin
HE	Haemagglutinin-esterase
HIV	Human immunodeficiency virus
IAV	Influenza A virus
L	Avogadro number = 6.022 × 10^{23} molecules per mol
K_{mucin}	Association constant for binding of virus to mucin at temperature T
$K_{a\_virus\_T}$	Association constant for binding of virus to host cells at temperature T
K_{d_mucin}	Dissociation constant for each CBD/SA interaction
$K_{d\_receptor\_T}$	Dissociation constant for GP from Cr at temperature T
LLF	Lung lining fluid
M	Molar (moles dm^{-3})
N_v	Number of GP/Cr contacts made on virus binding to cell
N_m	Number of GP/SA contacts made on virus binding to mucin molecule
MERS-CoV	Middle East respiratory syndrome coronavirus
MHV	Mouse hepatitis coronavirus
Muc_{free}	Number of free mucin molecules, i.e., not bound to virus
Muc_{total}	Total number of mucin molecules in given volume of mucus
NA	Neuraminidase
p_1	Probability of infection of host by exposure to a single virion
$p_{budding}$	Probability progeny virions exit the infected cell
p_{entry}	Probability that a virion bound to cell surface enters that cell
p_{cell}	Probability, given a virion has bound to the surface of a lung epithelial cell, that that cell becomes infected and releases its progeny viruses
p_{host}	Probability of successful infection of the host;
p_{pfu}	Probability that a given virion (represented in the exposure as a viral RNA copy) is itself capable of initiating infection in a cell
$p_{virogenesis}$	Probability virus replicates within cell after entry and progeny virions are assembled.
pfu	Plaque-forming unit
R	Ideal gas constant = 8.31 J/mol/K
$S1^A$	Head of CoV spike protein that binds SA
$S1^B$	Head of CoV spike protein that binds protein Cr
S2	Stalk of CoV spike protein involved in membrane fusion and virus entry
SARS-CoV	Severe acute respiratory syndrome coronavirus
ΔS_{a_immob}	Change in entropy on immobilization of whole virus on binding to cell surface
ΔS_{a_mucin}	Change in entropy on immobilization of whole virus on binding to mucin
SA	Sialic acid
TMPRSS	Transmembrane protease/serine protease that cleaves spike protein into S1 and S2
$V_{expsoure}$	Airborne exposure to a given dose of virions
V_{free}	Virus not bound to mucin molecules
V_{mucus}	Virus dose entering mucus in lung lining fluid
V.Muc	Number of viruses with bound mucin

$$p_{host} = 1 - (1 - p_1)^{V_{exposure}} \quad (1)$$

where p_1 is the probability of infection of the susceptible person by a single virion in an aerosol particle. Although Eq. 1 represents a dose-response for a set of equally susceptible individuals it is important to note that p_1 itself may vary between individuals within a population depending for example on genetic factors (Plante et al. 2020) and overall health of the individuals. This is addressed here for individuals

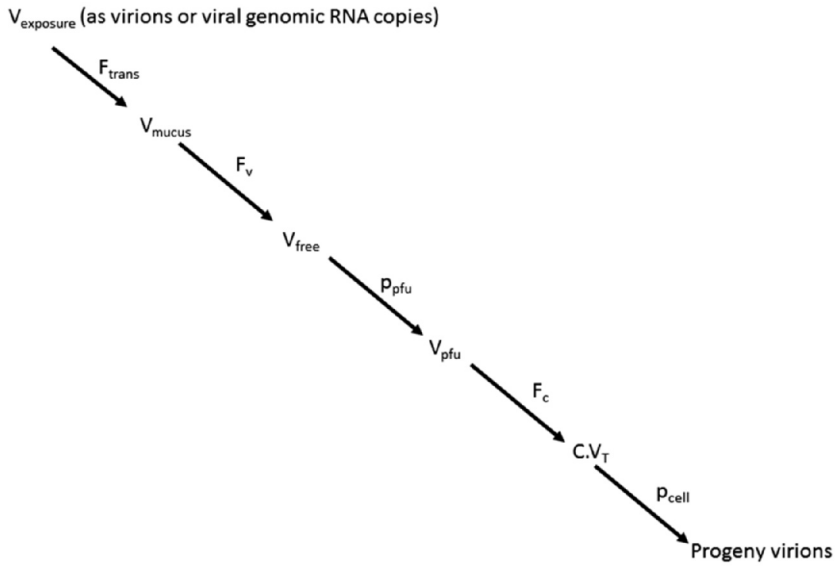

Fig. 1. Pathway from virus exposure to infection of cell.

with differing concentrations of mucin in the LLF.

At a cellular level, the probability of infection of the host, p_{host}, equals the probability of successful infection of at least one bronchus or lung cell and is related to the number of bronchus/lung cells ($C.V_T$) with bound virus by:-

$$\boldsymbol{p_{host}} = 1 - (1 - \boldsymbol{p_{cell}})^{C.V_T} \tag{2}$$

where p_{cell} is the probability of successful infection of a host bronchus/lung cell given a virus has bound to its surface. Thus the more bronchus/lung cells with bound virus then the greater the chance that infection will be successful in at least one of them. Based on the thermodynamic approach described previously (Gale 2018) and accommodating the fate and transport of the virions through the airways (Weir and Haas 2011) the development of the dose-response is broken down into five steps as shown in Fig. 1:-

1 Estimation of the fraction, F_{trans}, of the exposure dose, $V_{exposure}$, that is transported through the nasal airways to reach the mucus in the lung-lining fluid of the nasal epithelium/bronchus/lung;
2 Calculation of the number, V_{free}, of viruses getting through the host defences e.g. mucins and pathogen pattern recognition receptors to the lung epithelium. This is dependent on the fraction, F_v, of the total virions (V_{mucus}) in the mucus which are not bound to mucin;
3 Estimation of the probability, p_{pfu} that a given virion (represented in the exposure as a viral RNA genomic copy) is fit and actually capable at the molecular level of binding to and initiating infection in a susceptible host cell such that it could be detected as a pfu;
4 Calculation of $C.V_T$ as the fraction, F_c, of viruses bound to cells based on the thermodynamics of virus/host cell binding and in particular the number and strength of the virus glycoprotein (GP)/cell receptor (Cr) interactions together with the parameter ΔS_{a_immob}, which is the change in entropy on immobilization of whole virus on binding to the cell surface (Gale 2019; Gale, 2020); and
5 Estimation of the probability p_{cell} which depends on the ability of the bound virus to enter the cell, replicate and bud releasing progeny virions (Gale, 2017).

The total number, V_{free}, of viruses surviving the mucin barrier, and getting through to the lung epithelium from Fig. 1 is given by

$$\boldsymbol{V_{free}} = \boldsymbol{F_{trans}} \times \boldsymbol{F_v} \times \boldsymbol{V_{exposure}} \tag{3}$$

However, the $C.V_T$ term in Eq. 2 cannot be replaced by V_{free} calculated as Eq. 3 because $C.V_T$ should be an integer to represent a whole number of cells. As an alternative approach from Fig. 1, the probability, p_1, of infection of the host by exposure to a single virion in Eq. 1 may be expressed as

$$p_1 = F_{trans} \times F_v \times p_{pfu} \times F_c \times p_{cell} \tag{4}$$

since the F_{trans}, F_v and F_c terms may be interpreted as probabilities. Thus a prototype thermodynamic dose-response for a respiratory virus in humans is given by:-

$$p_{host} = 1 - (1 - (F_{trans} \times F_v \times p_{pfu} \times F_c \times p_{cell}))^{V_{exposure}} \tag{5}$$

It should be noted that the p_{pfu} term represents the fitness of the virion itself, while the p_{cell} term represents the ability of a host cell with bound (viable) virus to undertake and complete virogenesis. The two terms are completely unrelated.

2.3. Estimation of F_{trans}, the fraction of inhaled virions which are transported through the airways to reach the mucus in the lung lining fluid

Weir and Haas (2011) model anthrax spore transport through three regions of the respiratory system namely i) the nasal cavity and larynx, ii) the trachea and first branches of the bronchioles and iii) the respiratory bronchioles and alveoli. The model here for SARS-CoV-2 is based on cells within the lung and bronchioles expressing hACE2 being able to bind SARS-CoV-2 and on the basis of data from Hui et al. (2020) and Lukassen et al. (2020), SARS-CoV-2 only needs to get to the bronchus and does not need to reach the alveoli, unlike spores of *B. anthracis*, to initiate infection in a host. In the case of MERS-CoV which uses a different cell surface receptor from SARS-CoV-2, namely dipeptidyl peptidase 4 (DPP4 or CD26) and possibly certain glycans, cells of the bronchial submucosal glands and bronchus are targeted (Hui et al. 2020; Li et al. 2017). The prototype model presented here does not formally assess the fate and transport of the virus through the respiratory system as described by Weir and Haas (2011) for anthrax spores, and F_{trans} is set to 1 such that all the SARS-CoV-2 and MERS-CoV virions in the exposure are assumed to get to the mucus in the bronchus. This is justified for SARS-CoV-2 because recent evidence suggests that the nasal surfaces might be the dominant initial site for respiratory tract infection with likely subsequent aspiration-mediated virus seeding to the lung in SARS-CoV-2 pathogenesis (Hou et al. 2020). It is suggested here that determining F_{trans} is much more important for anthrax because once inhaled anthrax spores are infectious only after being transported to the alveoli (Weir and Haas 2011). According to

Hou et al. (2020) the nose contains the highest percentage of ACE2-expressing ciliated cells in the proximal airways with high SARS-CoV-2 infectivity of nasal epithelium and a gradient in infectivity characterized by a marked reduction in the distal lung (bronchioles and alveoli). As Hou et al. (2020) point out, aerosol deposition and fomite mechanical delivery deposition modelling suggest that aerosols containing virus inhaled by subjects achieve the highest density of deposition, i.e., highest viral loading per unit surface area, in the nose. This is completely different to the anthrax model and on the basis of the data of Hou et al. (2020) the prototype SARS-CoV-2 model here only needs to focus on the nasal epithelium.

2.4. Prediction of F_v, the fraction of viruses in the mucus layer which are free to bind to receptors on the lung epithelium

It is assumed that one virus binds to one mucin molecule to give a virus/mucin complex (V.Muc) in a dynamic equilibrium (Gale 2018).

$$V_{free} + Muc_{free} \leftrightarrow V.Muc$$

The strength of the binding is reflected by the association constant, K_{mucin}, between virus and mucin and is expressed as:-

$$K_{mucin} = \frac{[V{\cdot}Muc]}{[V_{free}][Muc_{free}]} \tag{6}$$

The fraction of free virus (F_v) is given by:-

$$\boldsymbol{F_V} = \frac{[\boldsymbol{V_{free}}]}{[V_{free}] + [\boldsymbol{V{\cdot}Muc}]} \tag{7}$$

Replacing [V.Muc] with Eq. 6 and rearranging gives F_v in terms of the free mucin concentration [Muc_{free}] and K_{mucin} in Eq. 8.

$$\boldsymbol{F_V} = \frac{1}{1 + \boldsymbol{K_{mucin}}[\boldsymbol{Muc_{free}}]} \tag{8}$$

2.4.1. Estimation of [Muc_{free}] in non-smokers

Kesimer et al. (2017) reported mean (± SE) concentrations of 108 ± 20 pmol per cm^3 for MUC5B and 10 ± 4 pmol per cm^3 for MUC5AC in lung mucus from persons who had never smoked. The mean concentration for MUC5AC plus MUC5B in non-smokers is therefore 118 pmol per cm^3, which is 1.18×10^{-7} M. Using the Avogadro number, L = 6.022×10^{23} molecules per mol, 118 pmol equates to 7.1×10^{10} molecules of MUC5AC and MUC5B in total per mm^3 volume of lung mucus.

2.4.2. Variation in lung mucin concentrations between individual non-smokers

It is important for a dose-response model to accommodate variation between indivduals in their susceptibility to infection. Kesimer et al. (2017) measured absolute concentrations of MUC5B and MUC5AC in 19 non-smoker participants and reported large variation between individuals. Thus although the mean [MUC5B] absolute concentration was 108 pmol/cm^3 the minimum was 20 pmol/cm^3 and the maximum was 300 pmol/cm^3.

2.4.3. Calculation of F_v for dispersed virus using Equation 8

The degree of localised dispersion of the virus in the mucus is an important consideration in the methodology in relation to calculation of [Muc_{free}] in Eq. 8. Where the virus is well dispersed in the lung mucus such that everywhere [V_{mucus}] << [Muc_{total}], then F_v can be calculated from Eq. 8 using [Muc_{total}] to approximate [Muc_{free}]. The fact that with $Muc_{total} >> V_{mucus}$ everywhere in the lung means that even with all the viruses in the initial challenge dose bound to mucin, $Muc_{free} \sim Muc_{total}$ and therefore [Muc_{total}] can be used to approximate [Muc_{free}] in Eq. 8. Thus [Muc_{free}] is set to 1.18×10^{-7} M in Eq. 8 for non-smokers.

2.4.4. Calculation of F_v for locally aggregated virus using the difference equation approach

When K_{mucin} is large and where [V_{mucus}] approaches or exceeds [Muc_{total}] locally, [Muc_{free}] becomes much smaller than [Muc_{total}] as the virus overwhelms and mops up all the free mucin molecules. In the extreme all the local mucins molecules are bound to virus and [Muc_{free}] tends to 0 locally. Therefore the difference equation approach has to be used as described previously (Gale 2018). Briefly K_{mucin} values are calculated using Eq. 6 for the range of V_{free}, Muc_{free} and V.Muc combinations from V.Muc = 1 to V.Muc = V_{mucus} (or to V.Muc = Muc_{total} depending on which is the lesser) assuming $Muc_{total} = 7.1 \times 10^{10}$ molecules of MUC5AC and MUC5B in total per mm^3 and converted to their respective concentrations [V_{free}], [Muc_{free}] and [V.Muc] by dividing by 10^{-6} dm^3/mm^3 and by L. The fraction of free virus, F_v, is then calculated as V_{free}/V_{mucus}.

2.4.5. Values of K_{mucin}

For the purpose of demonstration of the model, K_{mucin} values from 1 M^{-1} to 10^{22} M^{-1} are used. K_{mucin} is related to the number N_m of interactions between carbohydrate binding domains (CBDs) on the lectin (virus) and the SA glycans on the mucin according to:-

$$K_{mucin} = \frac{1}{(K_{d\_mucin})^{Nm}} \times e^{\frac{\Delta S_{a\_mucin}}{R}} \tag{9}$$

where K_{d_mucin} is the dissociation constant for each CBD/SA interaction, ΔS_{a_mucin} is the change in entropy on immobilization of whole virus on binding to mucin and R is the ideal gas constant (Gale 2018).

2.5. Modelling the effect of the virus:mucin ratio on the fraction, F_v, of free virus

Two scenarios are modelled for each virion:mucin ratio.

2.5.1. Scenario 1: Inhaled aerosol particles with different viral loads are each engulfed in 1 mm^3 of mucus

For the purpose of undertaking the difference equation approach a 1 mm^3 volume (10^{-6} dm^3) is chosen to represent the volume of mucus into which the virus dose (V_{mucus}) is dispersed as the airborne particle (s) enter(s) the LLF of the lung. This volume of mucus contains 7.1×10^{10} mucin molecules. It is assumed that virus doses of 2x, 1x, 0.5x and 0.1 × 7.1×10^{10} virions respectively (Table 2) are effectively exposed to the 7.1×10^{10} mucins in 1 mm^3 of mucus as they pass through the mucus to the lung epithelium. In effect the 1 mm^3 volume of mucus represents the limit of the aerosol dispersion in the mucus, such that within that 1 mm^3 volume as many virions as possible (given the dose) are exposed to mucins. It can be envisaged as providing the thinnest layer of mucus film that maximises the number of viruses in the dose that are in direct contact with mucus and hence exposed to a mucin. Eq. 6 is based on concentrations and K_{mucin} will be same whether it's calculated using 7.1×10^4 viruses and 7.1×10^4 mucins in a volume of 10^{-6} mm^3 for example or using 7.1×10^{10} virus and 7.1×10^{10} mucins in 1 mm^3 as performed here in the model. However, although a dose of 7.1×10^4 SARS-CoV-2 virions is perhaps more realistic as an inhaled dose based on $10^{8.94}$ virions per cm^3 of saliva (To et al. 2020), it is preferable to use values of 7.1×10^{10} virus and 7.1×10^{10} mucins in the difference equation approach to achieve the greater range of simulated K_{mucin} values and greater incremental sensitivity. So with 7.1×10^4 viruses and 7.1×10^4 mucins the highest K_{mucin} that can be achieved with the difference equation approach is $10^{16.6}$ M^{-1}. This compares to $10^{28.6}$ M^{-1} which can be achieved with 7.1×10^{10} viruses and 7.1×10^{10} mucins in 1 mm^3.

2.5.2. Scenario 2: Aerosol particles with the same viral load are each engulfed in different volumes of mucus

A dose of 7.1×10^{10} virions is locally dispersed into 0.5 mm^3 (representing 2 virions per mucin), 1 mm^3 (representing 1 virion per

Table 2
Fraction, F_v, of free virus in lung mucus calculated by difference equation approach for range of virion to mucin molecule ratios representing exposure of virion to mucins at the aerosol particle/mucus interface.

Scenario 1: Number of virions to number of mucin molecules in 1 mm^3 volume of mucus	Scenario 2: Number of virions to number of mucin molecules (volume of mucus)	Local ratio virion:mucin at aerosol particle/mucus interface	F_v at $K_{mucin} = 10^{10}\ M^{-1}$ (Reduction in risk by mucus)	F_v at $K_{mucin} = 10^{22}\ M^{-1}$.
1.42×10^{11} virions to 7.1×10^{10} mucins	7.1×10^{10} virions to 3.55×10^{10} mucins in 0.5 mm^3.	2:1	0.5004 (2-fold)	*0.5000
1.07×10^{11} virions to 7.1×10^{10} mucins	7.1×10^{10} virions to 4.73×10^{10} mucins in 0.666 mm^3.	1.5:1	0.334 (3-fold)	*0.333
7.1×10^{10} virions to 7.1×10^{10} mucins	7.1×10^{10} virions to 7.1×10^{10} mucins in 1 mm^3.	1:1	0.0286 (35-fold)	0.3×10^{-7}
3.55×10^{10} virions to 7.1×10^{10} mucins	7.1×10^{10} virions to 1.42×10^{11} mucins in 2 mm^3.	1:2	0.00169 (588-fold)	1.4×10^{-11}
$<0.71 \times 10^{10}$ virions to 7.1×10^{10} mucins	7.1×10^{10} virions to $>7.1 \times 10^{11}$ mucins in >10 mm^3.	<0.1:1 (Eq. 8)	0.00085 (1,176-fold)	$<10^{-15}$

*limit of what is achievable given ratio

mucin), 2 mm^3 (representing 1 virion per 2 mucins) and 10 mm^3 (representing 1 virion per 10 mucins) of lung mucus with $[Muc_{total}] = 1.18 \times 10^{-7}$ M.

2.6. Estimation of p_{pfu}, the probability that a virion (as represented by a viral RNA genomic copy) is capable of initiating infection in a cell

Not all virions produced during infection are capable of initiating infection in a subsequent host. Thus Bull et al. (2012) showed only 0.01% of norovirus particles could initiate infection in humans because each of the virions is different due to the mutant spectrum. According to Vicenzi et al. (2004) approximately 360 viral genomes of SARS-CoV are required to generate a pfu. This can be interpreted as 359 of every 360 virions being unable to initiate infection (non-infectious). Thus p_{pfu} is calculated as 1/360 = 0.0028.

2.7. Calculation of the fraction, F_c, of virus bound to cells from the association constant, $K_{a\_virus\_T}$ representing the strength of virus binding to host cells

Central to calculation of the number of lung epithelial cells with bound virus is the association constant, $K_{a\_virus\_T}$ which represents the strength of binding of whole virus to a lung cell at temperature T (Gale 2019, Gale, 2020). This is calculated as

$$K_{a\_virus\_T} = \frac{1}{(K_{d\_receptor\_T})^{N_v}} \times e^{\frac{\Delta S_{a\_immob}}{R}} \quad (10)$$

where $K_{d\_receptor\_T}$ is the dissociation constant for the CoV spike trimer protein from its proteinaceous cellular receptor, Cr, at temperature T, N_v is the number of spike protein trimer/Cr interactions on virus/host cell binding and ΔS_{a_immob} is the change in entropy on immobilization of whole virus on binding to the cell surface (Gale 2019, Gale, 2020).

2.7.1. Values of $K_{d\_receptor\_T}$ for SARS-CoV, SARS-CoV-2 and MERS-CoV

The dissociation constant, $K_{d\_receptor\_T}$ represents the strength of the interaction between the CoV spike protein and Cr with smaller values representing stronger binding. Wrapp et al. (2020) demonstrate that each SARS-CoV-2 trimer binds just one ACE2 with a $K_{d\_receptor\_T}$ of 1.47×10^{-8} M. This is much higher affinity binding than the $K_{d\_receptor\_T}$ of 1.85×10^{-7} M for the SARS-CoV spike trimer binding to a single ACE2 reported by Kirchdoerfer et al. (2018). The value of $K_{d\_receptor\_T}$ for each MERS spike protein binding to its CD26 (DPP4) cellular receptor is 1.67×10^{-8} M (Lu et al., 2013).

2.7.2. Values of N_v

There are on average 74 spike trimers per SARS-CoV virion (Neumann et al. 2011) each of which could in theory make at least one interaction with ACE2. According to Guo et al. (2018) 10% of the IAV virus surface could be in contact with a surface, such that approximately 7 IAV HA trimers can interact with receptor-loaded SA molecules. Thus N_v could be as high as 7 spike trimer protein/receptor contacts in the case of MERS-CoV, SARS-CoV and SARS-CoV-2 which are of similar size to IAV. Yuan et al. (2017) hypothesize that for MERS-CoV bound on the cell surface, one DPP4 receptor may crosslink two S trimers by binding to receptor-binding domains, one from each trimer thus giving large values for N_v involving multiple spike proteins linked together with DPP4 receptors.

2.7.3. Values of ΔS_{a_immob}

The parameter ΔS_{a_immob} was first identified in a thermodynamic analysis of the effect of temperature on virus binding to host cells (Gale 2019) and not surprisingly there are no data for its magnitude as yet although it is likely to be large and negative depending on the degree of immobilisation of the whole virus on binding to the host cell. The translational entropy of a particle of molecular weight 2.5×10^8 Da as for Rous sarcoma virus (Vogt and Simon 1999) is estimated to be

+350 J/mol/K using the Sackur-Tetrode equation (P. Gale unpublished results). Assuming half of this entropy is lost on cell binding and that the rotational entropy lost is similar (Finkelstein and Janin 1989) then ΔS_{a_immob} would approximate -350 J/mol/K although estimates based on Eq. 10 suggest values as low as -1,091 J/mol/K (Gale 2020). This large negative entropy change may be offset to some degree by non-specific attachment of the virus to the cell surface through SA and heparan sulphate binding as proposed for HIV such that much of the entropy loss of ΔS_{a_immob} on virus binding is taken prior to specific GP/Cr binding (Gale 2020). For the purpose of the prototype model developed here a value of -350 J/mol/K is used for ΔS_{a_immob}.

2.7.4. Demonstration that $F_c \sim 1$ in the lung model for $K_{a\_virus\_T} > \sim 10^{14}$ M^{-1}

The previous thermodynamic dose response models for virus binding in the human intestine (Gale 2018) and in the arthropod midgut (Gale 2019) have both shown that when $K_{a\_virus\_T}$ is $> \sim 10^{15}$ M^{-1} then its actual value is not important because at high virus doses all the host cells have bound virus while at low virus doses all the viruses are bound to host cells. This is therefore investigated for the lung model. Using the difference equation approach (Gale 2018) for binding of 1,000 virions in 25 cm^3 of LLF, the fraction, F_c, of virus dose bound to lung cells as a function of $K_{a\_virus\_T}$ was calculated for $C_{total} = 1.2 \times 10^9$ cells and for $C.V_T = 1$ to 1,000 (representing all viruses bound).

2.8. Estimation of p_{cell}

The parameter p_{cell} is the probability of viral entry (through fusion of the virus envelope with the host cell membrane) combined with the probabilities of each of the subsequent steps of virogenesis within the cell being completed, including viral polyprotein synthesis and cleavage by the virus-coded main protease (Zhang et al. 2020), viral RNA replication and capsid assembly followed by budding (viral egress) of progeny virions from the infected cell. Thus p_{cell} can be broken down into three conditional probabilities:-

$$p_{cell} = p_{entry} \times p_{virogenesis} \times p_{budding} \quad (11)$$

where p_{entry}, $p_{virogenesis}$ and $p_{budding}$ are the probabilities of entry of a bound virus into the cell interior, synthesis of the viral protein and RNAs within the cell and egress of the virus from the cell, respectively. Entry of the bound SARS-CoV-2 virion to the cell through fusion of the viral envelope with the host cell membrane is mediated by the spike protein S2 subunit which is conserved among coronaviruses (Walls et al. 2017). Cleavage at S1/S2 occurs upon biogenesis and viral egress for some coronaviruses, such as MHV and MERS-CoV (Walls et al. 2017). TMPRSS processing of SARS-CoV and MERS-CoV spike protein occurs at the cell membrane (Walls et al. 2017). Hoffmann et al. (2020) demonstrated efficient proteolytic processing of SARS-CoV-2 spike protein by TMPRSS2 in human kidney cell lines suggesting that fusion and entry should occur with high efficiency in human kidney cells at least, such that p_{entry} is high. The values for the probabilities $p_{virogenesis}$ and $p_{budding}$ for SARS-CoV-2 are also assumed to be high on the basis of ex vivo studies of SARS-CoV-2 infection in bronchus and lung cell cultures (Hui et al. 2020). It is assumed here that overall p_{cell} is highly efficient with a probability of 0.5 for the purpose of this prototype model.

3. Results

3.1. Increasing K_{mucin} decreases the fraction of free virus particularly at lower virus to mucin ratios

The predicted fractions of free virus and the efficacy of virus removal by the mucus barrier are presented for a range of virus:mucin ratios in Table 2 and plotted in Fig. 2 as a function of K_{mucin}. The results

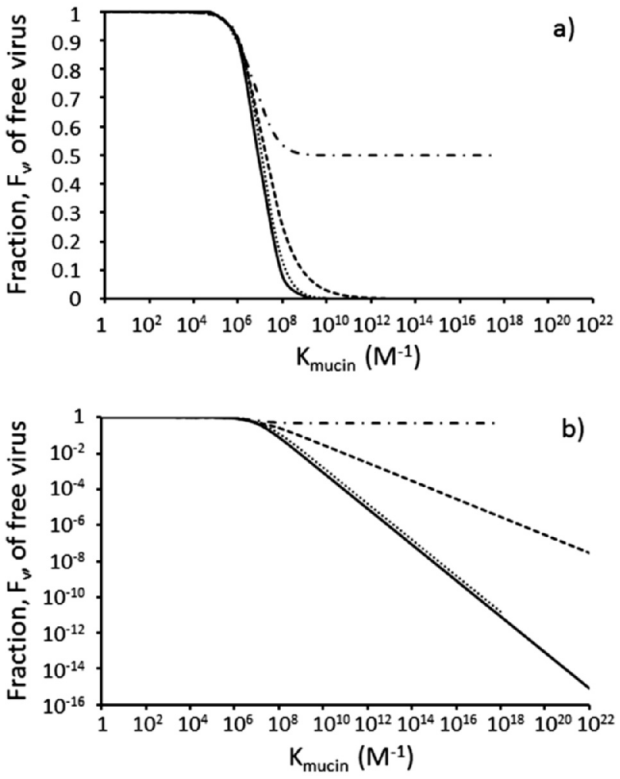

Fig. 2. The fraction, F_v, of free virus in mucus calculated by the difference equation approach decreases with increasing magnitude of the association constant, K_{mucin}, for binding of virus to mucin and is strongly affected by the local virus to mucin molecule ratio which is set to 2:1 (dash-dotted line), 1:1 (dashed line), 1:2 (dotted line) and <0.1:1 (solid line). The solid line is also represented by Eq. 8 for fully dispersed virus with $[Muc_{free}] = 1.18 \times 10^{-7}$ M. In a) the y-axis is linear to visualise the effect for the 2:1 virus:mucin ratio. In b) the y-axis is logarithm transformed to visualise small fractions of F_v as the virus becomes more dispersed in the mucus.

for Scenario 2 are identical to those for Scenario 1 in Table 2 which is not surprising since the values of $[V_{free}]$ and $[Muc_{free}]$ in the denominator of Eq. 6 are simply interchanged with the same [V.Muc] in the numerator. It is concluded that the results in Table 2 may be interpreted either in terms of challenge of a varying virus dose in a given fixed volume of mucus, or in terms of dispersion of a given fixed dose, V_{mucus}, of virions carried on an inhaled aerosol within differing "local micro-environment" volumes of the mucus in the LLF in the lung.

Low values of K_{mucin} have relatively little impact with F_v greater than 0.9 up to values of $K_{mucin} \sim 10^6$ M^{-1} (Fig. 2a) as expected for weak binding. At values of $K_{mucin} > 10^6$ M^{-1} values of F_v decrease significantly with increasing K_{mucin} (Fig. 2b). The decrease in F_v is enhanced with decreasing local virus:mucin ratio. For the highest virus:mucin ratio of 2:1, the value of F_v can never fall below 0.5 (Fig. 2a) irrespective of K_{mucin} because there is only sufficient mucin to mop up half of the virus dose, the other half of the virus dose remaining free to go on and infect lung epithelial cells. For virus:mucin ratios of 1:1 or less, Fig. 2b shows that above K_{mucin} of $\sim 10^6$ M^{-1} the fraction, F_v, of free virus decreases linearly with increasing K_{mucin}. The minimum value of F_v which is achievable at the 1:1 ratio is 1.4×10^{-11} reflecting just 1 in the 7.1×10^{10} viruses being free. This is not achieved for the 1:1 ratio even with a K_{mucin} as high as 10^{22} M^{-1} (dashed line in Fig. 2b). The minimum value of F_v which is achievable at the 1 virus:2 mucin ratio is 2.8×10^{-11} reflecting just 1 in the 3.55×10^{10} viruses being free. This is achieved at a K_{mucin} of 10^{18} M^{-1} and therefore the dotted line terminates at K_{mucin} $\sim 10^{18}$ M^{-1} (Fig. 2b). With the difference method approach it was not possible to achieve a K_{mucin} of $> 10^{18}$ M^{-1} for the 2 virus:1 mucin ratio simulation which is why the dash-dotted

line in Fig. 2 also terminates at K_{mucin} ~10^{18} M^{-1}. Using Eq. 8, values of F_v can be calculated for all values of K_{mucin} (solid line in Fig. 2b) and superimpose those for the 0.1 virion:1 mucin ratio.

3.2. Reducing the local virus:mucin ratio increases the efficiency of the mucus barrier

A K_{mucin} of 10^{10} M^{-1} is typical for lectins binding to mucins (see below). Table 2 presents the values of F_v over the range of local virion:mucin ratios for K_{mucin} = 10^{10} M^{-1}. At a local concentration of 2 virus to 1 mucin molecule, 50% of the virus is free such that the mucus barrier only reduces the risk by 2-fold. At a local ratio of 1:1, 2.9% of the virus is free representing a 35-fold reduction in risk by the mucus barrier, while decreasing the local ratio to 1 virus to 2 mucins reduced the free virus fraction to 0.17% representing a 588-fold reduction in risk by the mucus barrier. Fully dispersing the virus dose in the lung mucin such that the number of mucin molecules greatly exceeds the number of viruses reduces the fraction of free virus to 0.085% such that the risk is reduced almost 1,200-fold by the mucus barrier. These effects are even more marked for K_{mucin} of 10^{22} M^{-1} such that all the virus is bound at a ratio of 1 virus to 2 mucins (Table 2).

3.3. Modelling the number, $C.V_T$, of lung epithelial cells with bound virion

3.3.1. Most of the virus in the lung is predicted to be bound to cells at $K_{a\_virus\_T} > 10^{14}$ M^{-1}

The fraction, F_c, of virus bound to cells in the lung as a function of $K_{a\_virus\_T}$ is plotted in Fig. 3 and compared with the fractions of bound virus in the human intestine model (Gale 2018) and the mosquito midgut model (Gale 2019). Due to the higher concentration of target cells in the lung, lower values of $K_{a\_virus\_T}$ achieve greater virus binding than for the intestine and midgut models. Indeed 90% of the virus is bound to lung cells when $K_{a\_virus\_T} > 10^{14}$ M^{-1}. Thus F_c may be assumed to approximate 1 in Equation 5 if $K_{a\_virus\_T} > 10^{14}$ M^{-1}.

3.3.2. $K_{a\_virus\_T}$ is $> 10^{14}$ M^{-1} for the three CoVs if the number of trimer/receptor contacts is at least five

Values of $K_{a\_virus\_T}$ are calculated for SARS-CoV, SARS-CoV-2 and MERS-CoV using the reported $K_{d\_receptor\_T}$ values for the spike trimer binding and assuming ΔS_{a_immob} = -350 J/mol/K in Eq. 10 for four and five spike trimer/receptor interactions (Table 3). With N_v = 4 spike trimer/receptor contacts, values of $K_{a\_virus\_T}$ are well below 10^{14} M^{-1} while with N_v = 5 spike trimer/receptor contacts values of $K_{a\_virus\_T}$ are $>10^{14}$ M^{-1} for all three viruses.

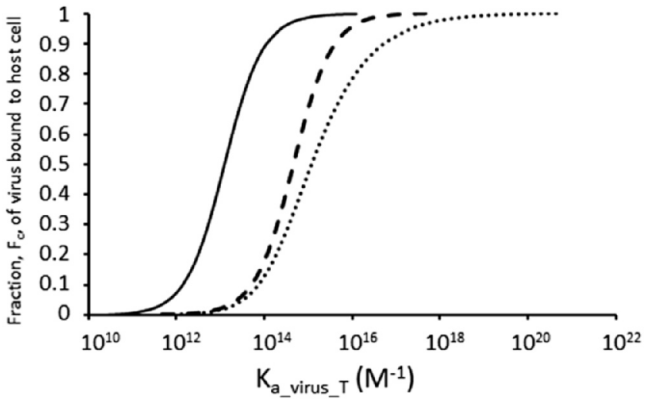

Fig. 3. The major proportion of virions is predicted to be bound to host cells in the human lung when $K_{a\_virus\_T}$ > ~10^{14} M^{-1}. Fraction, F_c, of virus dose of 1,000 virions predicted to be bound to host cells as a function of $K_{a\_virus\_T}$ for the human lung (solid line, C_{total} = 1.2 × 10^9 cells in 0.025 dm^3 of lung lining fluid, [C_{total}] = 8.0 × 10^{-14} M); human intestine (dashed line, C_{total} = 4.15 × 10^8 cells in 0.314 dm^3 of gut contents, [C_{total}] = 2.2 × 10^{-15} M) and mosquito midgut (dotted line, C_{total} = 1 × 10^3 cells in 10^{-6} dm^3 of midgut contents, [C_{total}] = 1.7 × 10^{-15} M) as calculated by the difference equation approach (Gale 2018).

Table 3
Values of $K_{a\_virus\_T}$ calculated for SARS-CoV, SARS-CoV-2 and MERS-CoV using the reported $K_{d\_receptor\_T}$ values (see text) for the spike trimer binding and assuming ΔS_{a_immob} = -350 J/mol/K (see text) in Eq. 10 for four and five spike trimer/receptor interactions.

	SARS-CoV	SARS-CoV-2	MERS-CoV
$K_{d\_receptor\_T}$ (M)	1.85 × 10^{-7}	1.50 × 10^{-8}	1.67 × 10^{-8}
$K_{a\_virus\_T}$ (M^{-1}) N_v = 4	4.36 × 10^8	1.01 × 10^{13}	6.57 × 10^{12}
$K_{a\_virus\_T}$ (M^{-1}) N_v = 5	2.36 × 10^{15}	6.73 × 10^{20}	3.93 × 10^{20}

3.4. Prototype dose-response model for initial infection in the lung by dispersed coronavirus

F_v values were calculated as 0.999, 0.894, 8.4 × 10^{-3}, and 8.47 × 10^{-6} for virus fully dispersed in lung mucus according to Equation 8 using [Muc_{total}] = 1.18 × 10^{-7} M and K_{mucin} values of 10^3 M^{-1}, 10^6 M^{-1}, 10^9 M^{-1} and 10^{12} M^{-1} to represent N_m = 1, 2, 3, and 4 contacts of K_{d_mucin} = 10^{-3} M, respectively (Eq. 9). These represent virus removals of 0.012%, 10.5%, 99.1% and 99.999% respectively. The probabilities, p_{host}, of infection over a range of virion exposures according to Equation 5 are compared for the four F_v values in Fig. 4. As expected from Fig. 2, increasing K_{mucin} from 10^3 M^{-1} to 10^6 M^{-1} representing a second additional spike protein/SA contact has little effect on reducing the infectivity. For these low values of K_{mucin}, the infectivity reflects the proportion of virions in the dose that are actually capable of initiating infection as represented by the value of p_{pfu} with predicted ID_{50}s of 498 virions (1.4 pfu) and 558 virions (1.6 pfu) for K_{mucin} values of 10^3 M^{-1} and 10^6 M^{-1} respectively (based on the assumed value of 0.5 for p_{cell}). However increasing K_{mucin} to 10^9 M^{-1} representing a third additional spike protein/SA contact increases the ID_{50} by ~100-fold to 59,243 virions (165 pfu) (Fig. 4). Increasing K_{mucin} by a further 1,000-fold to 10^{12} M^{-1} representing a forth additional spike protein/SA contact on binding with mucin increases the ID_{50} by 1,000-fold to ~5.87 × 10^7 virions (163,000 pfu) (Fig. 4). With a K_{mucin} value of 5 × 10^9 M^{-1} as for a lectin, F_v = 1.7 × 10^{-3} representing a 99.8% removal of the virus by the mucus giving an ID_{50} of 2.95 × 10^5 virions (819 pfu). Validation of the model in Fig. 4 for SARS-CoV-2 and MERS-CoV is not possible currently because there are no data for infectivity in humans. However, data for the proportion of dead mice after challenge by intranasal inoculation with increasing doses of SARS-CoV and MHV from Watanabe et al. (2010) are plotted as filled squares and open squares, respectively, in Fig. 4. The doses in units of pfu from Watanabe et al. (2010) have been converted to virions (or RNA genomic copies) by multiplying by $1/p_{pfu}$ for comparison with the model output here.

3.5. Estimation of values for p_1

From Equation 4, values for p_1, the risk of initial infection from exposure to a single virion, are 1.39 × 10^{-3}, 1.24 × 10^{-3}, 1.17 × 10^{-5}, 2.35 × 10^{-6} and 1.18 × 10^{-8} for K_{mucin} values of 10^3 M^{-1}, 10^6 M^{-1}, 10^9 M^{-1}, 5 × 10^9 M^{-1} and 10^{12} M^{-1} respectively with [Muc_{total}] = 1.18 × 10^{-7} M, thus completing the dose-response in Equation 1.

3.6. Predicted effect on efficiency of mucus barrier of variation between individuals in the concentrations of mucins in lung mucus

Assuming full dispersion in the mucus, the virus removals by the mucus barrier with a K_{mucin} value of 10^{10} M^{-1} ranged from 200-fold to

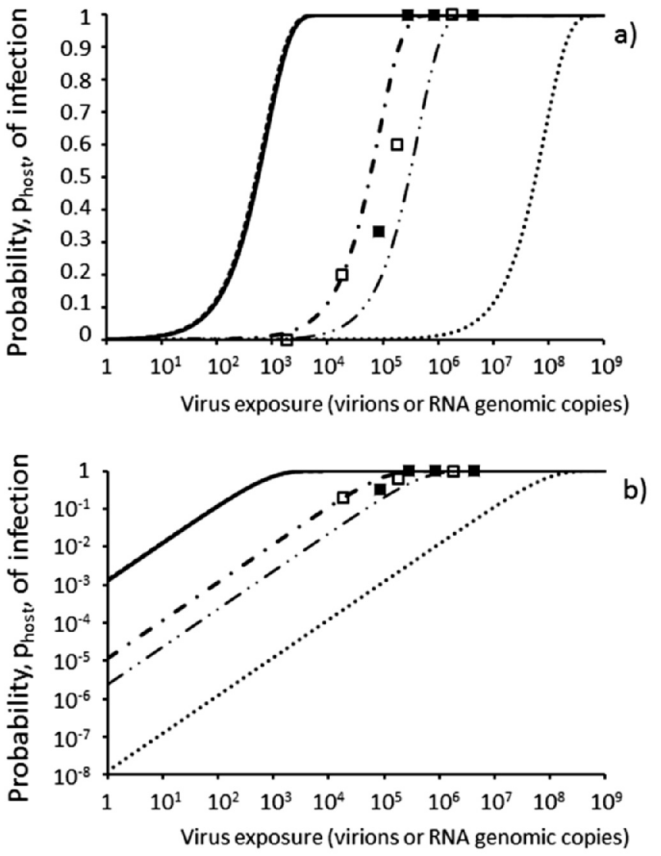

Fig. 4. Prototype dose-response models according to Equation 5 for respiratory coronavirus virion exposure with F_{trans} = 1, p_{pfu} = 0.0028, F_c = 1 and p_{cell} = 0.5. F_v values calculated with Equation 8 using $[Muc_{free}] \sim [Muc_{total}] = 1.18 \times 10^{-7}$ M assuming K_{mucin} values of 10^3 M^{-1} (dashed line), 10^6 M^{-1} (solid line), 10^9 M^{-1} (dash-dot line), and 10^{12} M^{-1} (dotted line) to represent N_m = 1, 2, 3, and 4 spike protein/mucin SA contacts, respectively, of $K_{d\_mucin} = 10^{-3}$ M (Eq. 9). Also $K_{mucin} = 5 \times 10^9$ M^{-1} (dash-dot-dot line) as for the lectin soy bean agglutinin binding to porcine submaxillary mucin (Dam and Brewer 2010). Squares represent proportion of mice which died after intranasal challenge of mouse hepatitis coronavirus (open) or SARS-CoV (filled) from Watanabe et al. (2010) assuming 1 pfu = 360 virions or genomic copies. In b) the y-axis is logarithm transformed to visualise risks from low doses of dispersed virus.

Table 4
Variation in absolute concentration of MUC5B in lung mucus from 19 non-smokers affects predicted efficiency of mucus barrier at removing respiratory viruses. MUC5B concentrations from Kesimer et al. (2017).

Participant	[MUC5B] (M)	F_v from Equation 8 ($K_{mucin} = 10^{10}$ M^{-1})	Overall removal of virus by mucus
Minimum	2.0×10^{-8}	0.005	201-fold
Mean	1.08×10^{-7}	0.000925	1,081-fold
Maximum	3.0×10^{-7}	0.000333	3,001-fold

3,000-fold as calculated by Equation 8 using minimum and maximum [MUC5B] reported by Keismer et al. (2017) for 19 non-smokers (Table 4). The variation between individuals in concentrations of MUC5B in lung mucus for non-smokers (Table 4) affects the dose-response with predicted ID_{50}s varying from 1.0×10^5 virions (278 pfu) up to 1.5×10^6 virions (4,160 pfu) with K_{mucin} at 10^{10} M^{-1} (Fig. 5).

4. Discussion

The work here builds on the thermodynamic approach developed previously for faecal/oral viruses in the human intestine (Gale 2018) and focuses on the fraction, F_v, of exposure dose, $V_{exposure}$, which is not bound to mucins in the lung mucus in the LLF and is therefore free to bind to and infect lung epithelial cells. Prototype dose-response models are plotted in Fig. 4 for a range of K_{mucin} values and in Fig. 5 to demonstrate the effect of varying $[Muc_{total}]$ in different individual non-smokers.

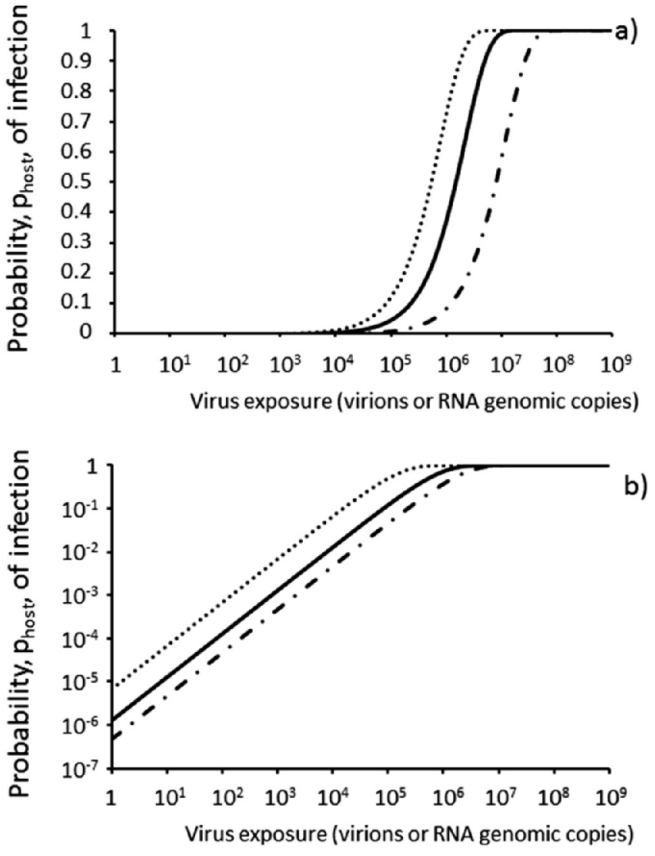

Fig. 5. Dose-response for respiratory coronavirus virion exposure varies between individuals depending on MUC5B concentration in the mucus (Table 4) according to Equation 5 (with F_{trans} = 1, p_{pfu} = 0.0028, F_c = 1 and p_{cell} = 0.5) for SARS-CoV-2 fully dispersed in lung mucus with $K_{mucin} = 10^{10}$ M^{-1} and F_v values calculated with Equation 8 using $[Muc_{free}] \sim [Muc_{total}] = 0.2 \times 10^{-7}$ M (dotted line), 1.08×10^{-7} M (solid line) and 3.0×10^{-7} M (dash-dot line).

The models in Fig. 4 and Fig. 5 represent the risk according to Equation 5 from virions which are fully dispersed in the mucus using F_v calculated with Equation 8. Equation 5 cannot be used with F_v values from Table 2 for aggregated virus doses (i.e. where local $V_{mucus} \geq Muc_{total}$) because F_v calculated by the difference equation approach is dependent on both the aggregation state of the virions and the number of virions in the inhaled aerosol particle, both of which affect the local virus:mucin ratio and hence $[Muc_{free}]$ (in Equation 8) where the aerosol interfaces with the mucus barrier.

The key conclusion of the prototype dose-response models is that dispersed SARS-CoV-2 virions are highly infectious to human without an effective mucus barrier in the lung with a predicted ID_{50} ~500 virions which equates to 1 to 2 pfu. This ID_{50} is dependent on the value of p_{pfu} which is given a point value of 0.0028 here based on 360 genomic copies per pfu. Adhikari et al. (2019) use a point value of 1,239 genomic copies per pfu for MERS-CoV based on SARS-CoV data and note the reported values ranged from 1:1 to 300:1 to 1,200-1,600:1. Using different point values would proportionately affect the number of virions comprising an ID_{50} and is a source of uncertainty addressed by Adhikari et al. (2019). The low ID_{50} values of 1 to 2 pfu for SARS-CoV-2 in the absence of effective mucin binding reflect both the tight binding

of the virion to the host cell through the high affinity spike protein/hACE2 interactions such that $K_{a\_virus\_T}$ is high (Table 3) and the efficient priming of the spike protein by proteolytic cleavage for fusion, such that p_{entry} is high. Increasing the magnitude of K_{mucin} as suggested here for MERS-CoV directly reduces the infectivity, such that with $K_{mucin} = 10^{12}\ M^{-1}$, the predicted $ID_{50} \sim 5.87 \times 10^7$ virions or 163,000 pfu. In terms of other applications, this prototype dose-response model may be used to test the effect of antiviral drugs on the infectivity. For example from drug inhibition data on the viral main protease (Zhang et al. 2020) it may be possible to model the effect of the drug on $p_{virogenesis}$ in Eq. 11 and hence assess the shift in dose response (Fig. 4) in the presence of the drug.

4.1. Fate and transport of the virions to the lung mucus

The dose response developed here is based on a virion dose being deposited in the mucus in the LLF in the bronchus and with $F_{trans} = 1$ in effect assumes 100% of the inhaled dose is deposited there. Deposition is a critical step in the initiation of infection by anthrax and varies between 9% and 30% of the inhaled dose depending on the host species (Gutting et al 2015). Specifically SARS-CoV-2 infects the nasal epithelium (Hou et al. 2020), the ciliated, mucus-secreting, and club cells of bronchial epithelium and the type 1 pneumocytes in the lung (Hui et al 2020). On the basis of the recent data of Hou et al. (2020) the model for SARS-CoV-2 only needs to focus on the nasal epithelium such that assuming $F_{trans} = 1$ may be justified. The prototype model here does not include lung air flow and pathogen transport principles as used in the anthrax model of Weir and Haas (2011). Instead, it is assumed that the fate of the virions deposited in the mucus in the LLF depends on whether each virion becomes bound subsequently to the mucins in the mucus and hence removed from the lung or remains free to bind to a host epithelial cell and initiate infection. This is accommodated in the F_v term, which is determined by both K_{mucin} and the mucin concentration according to Equation 8. To develop the model it may be possible to apply the fate and transport approaches developed by Weir and Haas (2011) to viruses using the K_{mucin} and mucin concentrations and also other diffusion approaches such as that developed for viruses moving through mucus (Erickson et al. 2015). A further difference between anthrax spores and SARS-CoV-2 is that cell tropism for the latter is dependent on the presence of the hACE2 receptor and the TMPRSS that cleaves spike protein into S1 and S2 (Lukassen et al. 2020; Hou et al. 2020). Although hACE2 and TMPRSS are expressed in cells from the lung and epithelial cells from the subsegmental bronchial branches, only a small proportion of cells express both (Lukassen et al. 2020) and are hence susceptible to SARS-CoV-2 infection. This is accommodated in the C_{total} term in this model which affects how F_c varies with $K_{a\_virus\_T}$ as shown for the human lung, human intestine and arthropod midgut models in Fig. 3.

4.2. The mucus barrier in the human lung may be more effective against MERS-CoV which binds human mucin than against SARS-CoV-2 which does not bind SA

It might be thought that the similarity of the dose-response data for MHV and SARS-CoV in the mouse data of Watanabe et al. (2010) presented as symbols in Fig. 4 argues against the importance of the mucus barrier in the thermodynamic dose-response model because the spike protein of MHV binds SA (Li et al 2017) while the spike protein of SARS-CoV-2 does not (Hao et al 2010). However, MHV differs from other CoVs in coding for an additional spike protein, the haemagglutinin-esterase (HE), which allows virions to elute from SA surfaces and hence provides the virions with a means of escape from irreversible attachment to non-cell-associated sialoglycoconjugates such as mucins (Langereis et al., 2011). Thus although MHV spike protein itself binds to SAs (Li et al. 2017) while SARS-CoV does not, the ability of the MHV to escape the mucin barrier would explain its similar dose-response in mice to SARS-CoV in the data of Watanabe et al. (2010) plotted in Fig. 4.

Adhikari et al. (2019) adopt the SARS-CoV dose-response model of Watanabe et al. (2010) as a surrogate for MERS-CoV in humans. However MERS-CoV may be different from SARS-CoV and SARS-CoV-2 in that it binds to human mucin through SAs (Li et al. 2017). More significantly it does not encode an HE protein (Du et al. 2017) with which to release itself from the SAs on the mucins (Langereis et al., 2011). Some beta-coronaviruses (as discussed for MHV above) do produce the HE protein which helps in the viral spread through the mucosa (Rabaan et al. 2020).Thus MERS-CoV may be effectively trapped by mucus in the human lung and according to the model here, this would increase the ID_{50} for MERS-CoV relative to that for SARS-CoV-2 and may contribute to explaining why MERS-CoV is less efficiently transmitted from person to person in the community.

4.3. Obtaining data on K_{mucin} for MERS-CoV and SARS-CoV-2 binding to mucins in human lung mucus

The results in Fig. 4 emphasise the potential of the mucus as a major barrier depending on the magnitude of the parameter K_{mucin}. Although SARS-CoV-2 does not bind to SAs (Hao et al. 2020), spike protein interactions with SA have been reported for several CoVs including MERS-CoV (Li et al. 2017). These interactions are mediated by the N-terminal domain ($S1^A$) of the spike protein while proteinaceous receptors (e.g. hACE2) are generally bound via $S1^B$ (Li et al. 2017). From Fig. 2a it can be seen that for the mucus to have any effect the magnitude of K_{mucin} must exceed $10^6\ M^{-1}$ and that K_{mucin} values of $10^{10}\ M^{-1}$ are required to achieve >1,000-fold removal of dispersed virus (Fig. 2b). Dam and Brewer (2010) report a K_{mucin} value of $5.0 \times 10^9\ M^{-1}$ for the lectin soy bean agglutinin binding to porcine submaxillary mucin which has multiple GalNAc sugars to bind. Similarly *Vataira macrocarpa* lectin has a K_{mucin} of $1.0 \times 10^{10}\ M^{-1}$ with porcine submaxillary mucin. Thus K_{mucin} values of $10^{10}\ M^{-1}$ used in the prototype dose response model (Fig. 4) may be realistic for MERS-CoV. Interactions between carbohydrate binding domains (CBDs) on proteins and monomeric SAs are generally weak with K_{d_mucin} values $\sim 10^{-3}$ M (Taylor and Drickamer, 2006; Fei et al. 2015) and indeed Li et al. (2017) describe the $S1^A$/SA interaction as weak for MERS-CoV. However, by making multiple contacts with the virus the affinity can be hugely increased according to Eq. 9 and Li et al. (2017) only detected MERS-CoV $S1^A$ binding to mucin when presented on nanoparticles such that multivalent (i.e. $N_m > 1$) CBD/SA interactions could be made thus enhancing binding affinity as expected from Eq. 9. For MERS-CoV the three $S1^A$ subunits of the spike trimer could each bind SA (i.e. one SA bound per S monomer). There are also 74 trimer spikes on each MERS-CoV virion (Neuman et al. 2011) so in theory there is potential for the virion to make multiple interactions with the multiple SAs on a mucin molecule such that K_{mucin} could become very large. Thus $N_m = 4$ CBD/SA interactions each of $K_{d\_mucin} = 10^{-3}$ M would give a K_{mucin} of $\sim 10^{12}\ M^{-1}$ according to Eq. 9. The magnitude of ΔS_{a_mucin} for immobilisation of the virus on the mucin surface in Eq. 9 is likely to be small because, unlike ΔS_{a_immob} for virus binding to a cell surface, binding to mucus is random.

Most mucins have a high SA content which, along with the high sulphate content, results in a strongly negative surface charge (Zanin et al. 2016). Hao et al. (2020) have shown that SARS-CoV-2 spike protein binds to heparan sulphate which also contains multiple sulphate groups. Moreover, basic amino acid residues (i.e. positively charged), known to constitute heparin binding domains are solvent accessible on the SARS-CoV-2 spike protein surface and form a continuous patch that is suitable for heparin binding (Mycroft-West et al. 2020). Human CoV NL63 also binds heparan sulphate which is used by this coronavirus for its attachment to target cells (Milewska et al 2014). This suggests SARS-CoV-2 and other human CoVs could bind to negatively charged groups on mucins despite not

binding to SAs (Hao et al. 2020). Thus binding of SARS-CoV and SARS-CoV-2 to human mucins will only be determined by experiment with human mucin itself and cannot be ruled out at this stage even though Hao et al. (2020) report it does not bind SA.

4.4. The degree of local dispersion/clustering of the virions in the lung mucus greatly affects the removal efficacy of the mucus

According to Scenario 2 in Table 2 inhalation of a fixed dose of SARS-CoV-2 virions dispersed across many aerosol particles may pose a greatly diminished risk compared to the same dose inhaled as a "cluster" in a single aerosol particle (providing $K_{mucin} \geq 10^{10}\ M^{-1}$). The virus:mucin ratio in Table 2 represents the local virion:mucin contact ratio and not the virus to mucin ratio across the whole 25 cm^3 of LLF which will be very low and representing an average. As the virus dose in the aerosol becomes more dispersed in the mucus then the local Muc_{total} begins to exceed V_{mucus} such that each virus is in effect surrounded by mucin molecules and has no contact or protective shielding effect from other viruses in the challenge dose from the aerosol particle. The model here suggests that the "local dilution" of a clustered virus dose from an aerosol only has to be ~>2-fold (Fig. 2) to almost maximise the effect of the protective mucus barrier. Thus according to the model each virus only needs to be surrounded by 2 mucin molecules of $K_{mucin} \geq 10^{10}\ M^{-1}$ in order to achieve a 588-fold reduction in risk of the virus getting to the epithelium and initiating infection. Infinite dilution as represented by the output of Equation 8 halves the risk again giving at the limit a 1,176-fold reduction in risk with <0.1% of the initial virus dose now free to bind to lung cells and initiate infection (Table 2).

4.5. The greatest change in risk occurs at the local virion/mucin ratio of 1:1 akin to a threshold

A four-fold increase in the local virus concentration in the mucus from 1 virion per 2 mucins to 2 virions per mucin gives ~300-fold increase in F_v (Table 2) and hence the risk of infection. This represents a co-operative effect within a virus "cluster" and breaks away from the traditional concept of independent action of pathogen infection although there is no absolute threshold effect in the model here. Bhar and Jones (2019) also challenge the "free independent virus particle" idea of viral transmission with the discovery of mechanisms by which multiple viral particles can infect the same cell simultaneously.

4.6. Impact of cell-tethered mucins is not considered here

The model here only considered the secreted mucins, MUC5B and MUC5AC, in the mucus and does not consider the cell-tethered mucins which may present an additional barrier to respiratory viruses. The cell-tethered mucins such as MUC1 and MUC4 form the basis of a gel-like layer surrounding the cilia (periciliary layer) that is essential for normal ciliary action to move mucus out of the airways (Ridley and Thornton 2018). The cell-tethered mucins provide a barrier function to mucosal pathogens by displaying sites for pathogen binding, acting as a releasable decoy, and sterically blocking binding of pathogens to underlying cellular receptors (McAuley et al. 2017). The cell-tethered mucin MUC1 gives protection against IAV H1N1 (McAuley et al. 2017). There is some evidence in mice that MUC4 gives protection to mice against SARS-CoV with $Muc4^{-/-}$ mice showing a modest 62% higher titre at 2 days post infection (dpi) and a 51% higher titre at 4 dpi as compared to wild type mice, although the increases were not statically significant (Plante et al. 2020). In contrast, $Muc1^{-/-}$ mice displayed a more rapid statistically significant rise in pulmonary IAV H1N1 loads compared to wild type mice at 1 to 3 dpi, although levels were comparable at 5 to 7 dpi (McAuley et al. 2017). Overall MUC4 offered protection to female mice against SARS-CoV and chikungunya virus pathogenesis although it was concluded this may not reflect a direct role such as the physical barrier function of mucin (Plante et al. 2020).

4.7. Uncertainty in the assumption that $F_c = 1$ i.e. all virus not bound to mucin is bound to lung epithelial cells

It is shown in Fig. 3 that >90% of the virus is bound to lung cells in the human lung model when $K_{a\_virus\_T}$ exceeds $10^{14}\ M^{-1}$, thus greatly simplifying the model because F_c in Equation 5 does not have to be calculated for each dose using the difference equation approach (Gale 2018) but can be assumed to approximate 1. While there is a published value of $K_{d\_receptor\_T}$ for SARS-CoV-2 spike trimer protein binding to a single hACE2 (Wrapp et al. 2020), there is no information on the number of contacts, N_v which must be at least five (Table 3) depending on ΔS_{a_immob} to ensure $K_{a\_virus\_T} > 10^{14}\ M^{-1}$ according to Eq. 10. According to Yang et al. (2005) HIV virions bearing IAV HA required 8 or 9 HA trimers for virus entry and Guo et al. (2018) suggest that approximately 7 IAV HA trimers can interact with receptor-loaded SA molecules. It is concluded that although there is considerable uncertainty in the exact value of N_v for SARS-CoV-2 and MERS-CoV it is likely to be greater than 4 for both and on the basis that N_v could be as high as 7 spike trimer protein/receptor interactions it is concluded that $K_{a\_virus\_T}$ is $>10^{14}\ M^{-1}$ according to Eq. 10 such that F_c can be assumed to approximate 1. This is in agreement with Walls et al. (2020) who suggest the observed tight binding of SARS-CoV-2 $S1^B$ to hACE2 could partially explain the efficient transmission of SARS-CoV-2 in humans.

It should also be noted that ΔS_{a_immob} in Eq. 10 is an unknown parameter for any virus and depends on the size of the virus (Gale 2019; Gale, 2020) together with how restricted virion mobility is on attachment to a host cell. The ΔS_{a_immob} of –350 J/mol/K used in Table 3 is estimated using the Sackur-Tetrode equation. A less negative ΔS_{a_immob} at –170 J/mol/K for example would require just three GP/Cr contacts to achieve $K_{a\_virus\_T}$ of $>10^{14}\ M^{-1}$ for SARS-CoV-2 according to Eq. 10 and ultimately it would be better to measure $K_{a\_virus\_T}$ experimentally if possible.

4.8. The host cell infection component of the prototype dose-response for SARS-CoV-2 is defined solely by cell binding and entry

As a probability, p_{cell}, can take a value between 0 (cell is refractory) and 1 (cell is fully permissive) and a value of 0.5 is assigned here on the basis of the efficiency of cleavage of SARS-CoV-2 spike protein by human cells (Hoffmann et al. 2020). The values of $p_{virogenesis}$ and $p_{budding}$ are assumed to ~1 in the calculation of p_{cell} in Eq. 11. In effect therefore the component of the dose-response for SARS-CoV-2 infection of human lungs is based solely on $K_{d\_receptor\_T}$, N_v and p_{entry}. This appears to be acceptable for assessing the zoonotic potential of bat CoVs. Thus Menachery et al. (2020) argue that the combination of receptor binding and proteolytic activation by endogenous proteases permits zoonotic CoV infection as with MERS-CoV and SARS-CoV, and can be used to evaluate zoonotic virus populations in bats for emergence threats. There are several human host cell proteases that can cleave the spike protein. Thus SARS-CoV can use the endosomal cysteine proteases cathepsin B and L and the serine protease TMPRSS2 for S protein priming in cell lines, and inhibition of both proteases is required for robust blockade of viral entry (Hoffmann et al. 2020). However, only TMPRSS2 activity is essential for SARS-CoV viral spread and pathogenesis in the infected host whereas CatB/L activity is dispensable (Hoffmann et al. 2020). Therefore p_{entry} should be based on the probability of cleavage by TMPRSS2 in order to model for spread of the virus in the body.

4.9. Comparing the prototype thermodynamic dose-response model for initial infection with published dose-response data for coronavirus death in mice

Although the K_{mucin} value from Dam and Brewer (2010) of 5×10^9

M^{-1} for lectin binding to porcine submaxillary mucin gives a good approximations to the MHV and SARS-CoV mouse death data (symbols in Fig. 4), this is not evidence of validation of the model here because MHV escapes mucin and SARS-CoV does not bind mucin and thus K_{mucin} values would be expected to be very small (certainly $<10^6$ M^{-1}) such that the predicted dose-response curve for initial infection by MHV and SARS-CoV in mice (solid line in Fig. 4) would have ID_{50}s of ~500 virions (1 to 2 pfu) according to the model here. It should be stressed that the data of Watanabe et al. (2010) as represented by the symbols in Fig. 4 are not comparable with the model outputs here, the former representing death while the latter represents initial infection of one or more epithelial cells in the nose or bronchus, with no inclusion of the effect of the innate immune response which is important in disease progression and illness in CoV infection (Lim et al. 2016). It is therefore not surprising that the ID_{50} for death (symbols) is higher than the ID_{50} for infection with low K_{mucin} (solid line) in Fig. 4.

4.10. Is the dose-response for SARS-CoV a good surrogate for SARS-CoV-2?

Although similar, there are some notable differences between the SARS-CoV-2 and SARS-CoV spike proteins (Rabaan et al. 2020; Wrapp et al. 2020). The key amino acid residues involved in ACE2 binding are largely different and the SARS-CoV-2 trimer binds to ACE2 with a ~12-fold lower $K_{d\_receptor\_T}$ than that of the SARS-CoV trimer (Table 3). The binding of SARS-CoV-2 is predicted to be much stronger than for SARS-CoV according to $K_{a\_virus\_T}$ values as the number of spike trimer/ACE2 contacts increase (Table 3). According to the model here in Fig. 3 this difference could be overcome by a sufficient number, N_v, of spike trimer/hACE2 contacts such that $K_{a\_virus\_T}$ exceeds 10^{14} M^{-1} (Table 3). However, the TMPRSS cleavage site in the spike protein sequence of SARS-CoV-2 may also account for the increased infectivity of SARS-CoV-2 relative to SARS-CoV (Hao et al 2020; Rabaan et al. 2020) such that p_{cell} may be lower for SARS-CoV than for SARS-CoV-2. Thus the dose-response of Watanabe et al. (2010) based on SARS-CoV and MHV in mice may not be appropriate for SARS-CoV-2 although in the absence of data it is used as a surrogate dose-response in airborne risk assessment (Buonanno et al. 2020).

4.11. Both SARS-CoV and MHV bind to host cells with high affinity consistent with similar dose-response models in mice

Although each SARS-CoV spike trimer could bind three ACE2 receptors, the stoichiometry of spike trimers binding ACE2 is complicated for SARS-CoV (Kirchdoerfer et al. 2018) with most trimers just binding one ACE2. This is because the three copies of SARS-CoV $S1^A$ protein which bind ACE2 are all located on the top of the spike trimer and are near each other, leading to steric clashes between bound ACE2 molecules (Shang et al. 2020). This contrasts with mouse hepatitis coronavirus (MHV) for which three receptor molecules bind to the sides of the spike trimer, where there is no steric clash (Shang et al. 2020). Thus each MHV trimer binds three receptors (Kirchdoerfer et al. 2018) and depending on the number of receptor molecules on host cell membranes, Shang et al. (2020) conclude that the high stoichiometry of receptor binding by MHV spike potentially allows efficient viral attachment to target cells. Thus in addition to not being bound by mucins, both MHV and SARS-CoV could attach to host cells with high affinity consistent with their similar dose-response curves for death in mice (symbols in Fig. 4).

4.12. Limitations of the model developed here

In addition to lack of data on the magnitude of K_{mucin} for viruses associating with mucins, current understanding of mucin functions is limited. This is partly due to the complexity of mucus and its interactions (Zanin et al. 2016). The interaction between mucins and respiratory pathogens is also more complicated than mere entrapment (Zanin et al. 2016). The model here only considers entrapment of the virus, and does not consider mechanisms for the virus to evade the mucus which do not appear to be known for CoVs. Although mucus is an important host barrier to IAV, the neuraminidase (NA) protein of IAV is important in evading this barrier, such that viruses with low NA activity, or viruses treated with NA inhibitors, are severely impeded by mucus in vitro (Zanin et al. 2016). Another limitation of the model is that it is possible that more than one virus can bind a mucin molecule since each mucin molecule has multiple SAs (Zanin et al. 2016).

According to Guo et al. (2018) equilibrium binding models (such as those developed here) are poorly applicable to the IAV-receptor interaction because the virus rolls over a surface (such as a host cell) coated with receptors enabled by NA activity. Migration of attached IAV particles over a receptor coated-surface depends on the very high $K_{d\_receptor\_T}$ (0.0003 to 0.003 M) values (i.e. low affinity binding) of monovalent HA/SA interactions resulting in their rapid formation and dissociation. Guo et al. (2018) hypothesize that NA, in combination with the highly dynamic formation and release of individual HA-SA interactions, drives virus rolling by the generation of a receptor gradient due to the receptor destroying activity of NA. This is a different strategy from SARS-CoV-2 cell binding for which $K_{d\_receptor\_T}$ for the trimer is very low at 1.5×10^{-8} M (Wrapp et al. 2020) and SARS-CoV-2 and MERS-CoV do not appear to utilize enzymes for viral release with only group 2a coronaviruses (human CoV-HKU1, MHV) having haemagglutinin esterases (de Groot 2006). It is concluded that the equilibrium binding models (such as those used here and previously (Gale 2018)) are applicable to coronaviruses, although not for IAV virions which have both HA and NA present in their viral envelopes. It may also not be applicable to MHV which also has HE.

4.13. The role of sialic acids: ΔS_{a_immob} vs K_{mucin}

Unlike IAV which only binds SA receptors, the spike protein trimers of CoV bind to protein Cr receptors with very high affinity. This raises the question of why some CoV spike proteins e.g. MERS-CoV, also bind to SAs, which according to the model here would hinder their movement through the mucus barrier. Other viruses also use non-specific attachment factors that bind the virus on the cell surface without initiating endocytosis and viral entry, for which specific receptors are required. In the case of tick-borne encephalitis virus, HIV, pseudorabies virus, sindbis virus, Semliki Forest virus, hepatitis E virus and Rift Valley fever virus the attachment factor is heparan sulphate, a negatively-charged glycosaminoglycan (Pulkkinen et al. 2018). SARS-CoV-2 spike protein also binds heparan sulphate (Hao et al., 2020). It was previously proposed that the attachment factors including cell surface SAs and heparan sulphate serve to take some of the entropy loss of ΔS_{a_immob} on virus binding (Gale 2020). Specifically for MERS-CoV, Li et al. (2017) provide evidence that SAs may serve as low-affinity attachment receptors and thereby aid viral entry through increasing the likelihood of MERS-CoV spike engagement with the DPP4 entry receptor. Thus the potential loss of the virus through binding to SAs on mucins in the mucus as suggested by the model here may be a trade-off for non-specific binding of viral spike proteins to SAs on the cell surface in overcoming the unfavourable ΔS_{a_immob}. In this respect, the magnitude of K_{mucin} in the F_v term plays off against that of ΔS_{a_immob} in the F_c term in Fig. 1.

5. Conclusions

The conclusions are:-

1 The outline of a thermodynamic equilibrium model for a dose-response for SARS-CoV-2 and MERS-CoV is set out here based on molecular parameters. The available parameters for the spike trimer/cell receptor interactions suggest the association constant for virus binding to a human bronchus/lung cell will be so high that any

virion getting through the mucus barrier will bind to these cells resulting in entry through spike protein fusion which is also known to be efficient for both viruses.

2 It is known that mucin proteins in lung mucus present a barrier to respiratory viruses. According to the model outlined here, the mucus in the 25 cm^3 volume of lung lining fluid could present a significant barrier to infection of lung cells in humans by coronaviruses if the magnitude of the association constant (K_{mucin}) defining the strength of binding of the virion to human mucin is at least 10^9 M^{-1} (as has been reported for lectins' binding to mucins).

3 The magnitude of K_{mucin} is currently unknown for any virus to the author's knowledge. While SARS-CoV-2 spike protein does not bind sialic acid, the spike protein of MERS-CoV does and indeed MERS-CoV has been shown to bind human mucin. A K_{mucin} of at least 10^{10} M^{-1} could theoretically be achieved for MERS-CoV with four low affinity contacts between virus spike protein and monomeric sialic acids on the mucin each with dissociation constants of $\sim 10^{-3}$ M (which is typical for carbohydrate binding domains on proteins binding to monomeric sialic acids). This could contribute to more efficient removal of MERS-CoV by the mucus barrier in the lung and hence its reduced human-to-human transmission compared to SARS-CoV-2. However SARS-CoV-2 spike protein has positively charged groups which could interact with negatively charged acidic groups on the mucins and its binding to human mucin cannot be ruled out without definitive data.

4 The mucus barrier may be more effective against fully dispersed virions in the case of MERS-CoV that binds human mucin. Some coronaviruses use an esterase to escape the mucin, although MERS-CoV does not. Instead, it is shown here that “clustering” of virions into single aerosol particles as recently reported for rotavirus in extracellular vesicles could provide a co-operative mechanism whereby MERS-CoV could theoretically overcomes the mucin barrier locally. In this respect the rare, high virion-load aerosol particles may be more important for transmission of MERS-CoV.

5 Assuming efficient transport to the mucus in the lung bronchus (or nasal epithelium in the case of SARS-CoV-2) and depending on the viability of individual virions, the ID_{50} for SARS-CoV-2 initial infection is estimated to be ~500 virions (viral RNA genomic copies) representing 1 to 2 pfu. Assuming a K_{mucin} of 5×10^9 M^{-1} as for lectin/mucin binding, the ID_{50} for MERS-CoV initial infection is estimated to be ~295,000 virions (viral RNA genomic copies) representing 819 pfu.

6 The thermodynamic equilibrium approach developed here based on virus binding to mucins according to K_{mucin} and the mucin concentration in mucus could complement inhalation models based on fate and transport as for anthrax spores in the lungs.

7 It is proposed that K_{mucin} is the cost for binding of viruses to sialic acids on the cell surface to partially overcome the unfavourable entropy of immobilisation of a virus.

Author Statement

I wrote this paper based on my previous thermodynamic dose-response models with no funding. It is my contribution to the global response against COVID-19.

Disclaimer

The views expressed in this paper are those of the author and not necessarily those of any organisations.

Declaration of Competing Interest

None declared.

References

Adhikari, U., Chabrelie, A., Weir, M., Boehnke, K., McKenzie, E., Ikner, L., Wang, M., Wang, Q., Young, K., Haas, C.N., Rose, J., Mitchell, J., 2019. A case study evaluating the risk of infection from Middle Eastern Respiratory syndrome coronavirus (MERS-CoV) in a hospital setting through bioaerosols. Risk Analysis 39, 2608–2624.

Anon (2020). Coronavirus resource center (https://coronavirus.jhu.edu/map.html) Accessed 8 August 2020.

Bhar, S., Jones, M.K., 2019. In Vitro Replication of Human Norovirus. Viruses 11 547. https://doi.org/10.3390/v11060547.

Bull, R.A., Eden, J.-S., Luciani, F., McElroy, K., Rawlinson, W.D., White, P.A., 2012. Contribution of intra- and interhost dynamics to norovirus evolution. Journal of Virology 86, 3219–3229.

Buonanno, G.L, Stabile, L, Morawska, L., 2020. Estimation of airborne viral emission: Quanta emission rate of SARS-CoV-2 for infection risk assessment. Environment International 141, 105794.

Crapo, J.D., Barry, B.E., Gehr, P., Bachofen, M., Weibel, E.R., 1982. Cell number and cell characteristics of the normal human lung. The American review of respiratory disease 126, 332–337.

Dam, T.K., Brewer, C.F., 2010. Oligosaccharide multivalent lectin–carbohydrate interactions: Energetics and mechanism of binding. Advances in Carbohydrate Chemistry and Biochemistry 63, 139–164.

De Graaf, M., Fouchier, R.A.M., 2014. Role of receptor binding specificity in influenza A virus transmission and pathogenesis. The EMBO Journal 33, 823–841.

De Groot, R.J., 2006. Structure, function and evolution of the hemagglutinin-esterase proteins of corona- and toroviruses. Glycoconj 23, 59–72.

Du, L., Yang, Y., Zhou, Y., Lu, L., Li, F., Jiang, S., 2017. MERS-CoV spike protein: a key target for antivirals. Expert Opin Ther Targets 21, 131–143.

Erickson, A.M., Henry, B.I., Murray, J.M., Klasse, P.J., Angstmann, C.N., 2015. Predicting first traversal times for virions and nanoparticles in mucus with slowed diffusion. Biophysical Journal 109, 164–172.

Fei, Y., Sun, Y.-S., Li, Y., Yu, H., Lau, K., Landry, J.P., Luo, Z., Baumgarth, N., Chen, X., Zhu, X., 2015. Characterization of receptor binding profiles of influenza A viruses using an ellipsometry-based label-free glycan microarray assay platform. Biomolecules 5, 1480–1498.

Finkelstein, A.V., Janin, J., 1989. The price of lost freedom: entropy of bimolecular complex formation. Protein Eng 3, 1–3.

Fröhlich, E., Mercuri, A., Wu, S., Salar-Behzadi, S., 2016. Measurements of Deposition, Lung Surface Area and Lung Fluid for Simulation of Inhaled Compounds. Front. Pharmacol 7, 181. https://doi.org/10.3389/fphar.2016.00181.

Gale, P., 2018. Using thermodynamic parameters to calibrate a mechanistic dose-response for infection of a host by a virus. Microbial Risk Analysis 8, 1–13.

Gale, P., 2019. Towards a thermodynamic mechanistic model for the effect of temperature on arthropod vector competence for transmission of arboviruses. Microbial Risk Analysis 12, 27–43.

Gale, P., 2020. How virus size and attachment parameters affect the temperature sensitivity of virus binding to host cells: Predictions of a thermodynamic model for arboviruses and HIV. Microbial Risk Analysis. https://doi.org/10.1016/j.mran.2020.100104.

Guo, H., Rabouw, H., Slomp, A., Dai, M., van der Vegt, F., van Lent, J.W.M., McBride, R., Paulson, J.C., de Groot, R.J., van Kuppeveld, F.J.M., de Vries, E., de Haan, C.A.M, 2018. Kinetic analysis of the influenza A virus HA/NA balance reveals contribution of NA to virus-receptor binding and NA-dependent rolling on receptor-containing surfaces. PloS Pathog 14 (8), e1007233.

Gutting, B.W., Rukhin, A., Mackie, R.S., Marchette, D., Thran, B., 2015. Evaluation of inhaled versus deposited dose using the exponential dose-response model for inhalational anthrax in nonhuman primate, rabbit, and guinea pig. Risk Analysis 35, 811–827.

Hao, W., Ma, B., Li, Z., Wang, X., Gao, X., Li, Y., Qin, B., Shang, s., Cui, S. and Tan, Z. (2020) Binding of the SARS-CoV-2 spike protein to glycans.

Hoffmann, M., Kleine-Weber, H., Schroeder, S., Kruger, N., Herrler, T., Erichsen, S., Schiergens, T.S., Herrler, G., Wu, N.-H., Nitsche, A., Muller, M.A., Drosten, C., Pohlmann, S., 2020. SARS-CoV-2 Cell Entry Depends on ACE2 and TMPRSS2 and Is Blocked by a Clinically Proven Protease Inhibitor. Cell 181, 1–10.

Hou, Y.J., Okuda, K., Edwards, C.E., Martinez, D.R., Asakura, T., Dinnon, K.H., Kato, T., Lee, R.E., Yount, B.L., Mascenik, T.M., Chen, G., Olivier, K.N., Ghio, A., Tse, L.V., Leist, S.R., Gralinski, L.E., Schäfer, A., Dang, H., Gilmore, R., Nakano, S., Sun, L., Fulcher, M.L., Livraghi-Butrico, A., Nicely, N.I., Cameron, M., Cameron, C., Kelvin, D.J., de Silva, A., Margolis, D.M., Markmann, A., Bartelt, L., Zumwalt, R., Martinez, F.J., Salvatore, S.P., Borczuk, A., Tata, P.R., Sontake, V., Kimple, A., Jaspers, I., O'Neal, W.K., Randell, S.H., Boucher, R.C., Baric, R.S., 2020. SARS-CoV-2 Reverse Genetics Reveals a Variable Infection Gradient in the Respiratory Tract. Cell 182, 429–446.

Huang, Y. (2013). SARS: Dose response models. Retrieved from http://qmrawiki.canr.msu.edu/index.php/SARS:_Dose_Response_Models#_9f6e9f18777d09a3e4569b0d5784d92f.

Hui, K.P.Y., Cheung, M.-C., Perera, R.A.P.M., Ng, K.-C., Bui, C.H.T., Ho, J.C.W., Ng, M.M.T., Kuok, D.I.T., Shih, K.C., Tsao, S.-W., Poon, L.L.M., Peiris, M., Nicholls, J.M., Chan, M.C.W., 2020. Tropism, replication competence, and innate immune responses of the coronavirus SARS-CoV-2 in human respiratory tract and conjunctiva: an analysis in ex-vivo and in-vitro cultures. The Lancet. https://doi.org/10.1016/S2213-2600(20)30193-4.

Kesimer, M., Ford, A.A., Ceppe, A., Radicioni, G., Cao, R., Davis, C.W., Doerschuk, C.M., Alexis, N.E., Anderson, W.H., Henderson, A.G., Barr, R.G., Bleecker, E.R., Christenson, S.A., Cooper, C.B., Han, M.K., Hansel, N.N., Hastie, A.T., Hoffman, E.A.,

Kanner, R.E., Martinez, F., Paine, III, R, Woodruff, P.G, O'Neal, W.K, Richard C. Boucher, R.C, 2017. Airway Mucin Concentration as a Marker of Chronic Bronchitis. N Engl J Med 2017 377, 911–922.
Killerby, M.E., Biggs, H.M., Midgley, C.M., Gerber, S.I., Watson, J.T., 2020. Middle East respiratory syndrome coronavirus transmission. Emerging Infectious Diseases 26, 191–198.
Kirchdoerfer, R.N., Wang, N., Pallesen, J., et al., 2018. Stabilized coronavirus spikes are resistant to conformational changes induced by receptor recognition or proteolysis. Sci Rep 8 (1), 15701.
Langereis, M.A., van Vliet, A.L., Boot, W., de Groot, R.J., 2011. Attachment of mouse hepatitis virus to O-acetylated sialic acid is mediated by hemagglutinin-esterase and not by the spike protein. Journal of Virology 84, 8970–8974.
Li, W., Hulswit, R.J.G., Widjaja, I., Rajb, V.S., McBride, R.Pengc,W., Widagdo, W., Tortorici, M.A., van Dieren, B., Lang, Y., Lent, J.W.M., Paulson, J.C., de Haan, C.A.M., de Groot, R.J., van Kuppeveld, F.J.M., Haagmans, B.L., Bosch, B.-J., 2017. Identification of sialic acid-binding function for the Middle East respiratory syndrome coronavirus spike glycoprotein. Proc. Natl. Acad. Sci. USA 114 (40), E8508–E8517.
Lim, Y.X., Ng, Y.L., Tam, J.P., Liu, D.X., 2016. Human coronaviruses: A review of virus–host interactions. Diseases 4, 26.
Lindsley, W.G., Pearce, T.A., Hudnall, J.B., Davis, K.A., Davis, S.M., Fisher, M.A., Khakoo, R., Palmer, J.E., Clark, K.E., Celik, I., Coffey, C.C., Blachere, F.M., Beezhold, D.H., 2012. Quantity and size distribution of cough-generated aerosol particles produced by influenza patients during and after illness. J. Occup. Environ. Hyg. 9, 443–449.
Lu, G., Hu, Y., Wang, Q., Qi, J., Gao, F., Li, Y., Zhang, Y., Zhang, W., Yuan, Y., Bao, J., Zhang, B., Shi, Y., Yan, J., Gao, G.F., 2013. Molecular basis of binding between novel human coronavirus MERS-CoV and its cellular receptor CD26. Nature 500, 227–231.
Lukassen, S., Chua, R.L., Trefzer, T., Kahn, N.C., Schneider, M.A., Muley, T., Winter, H., Meister, M., Veith, C., Boots, A.W., Hennig, B.P., Kreuter, M., Conrad, C., Eils, R., 2020. SARS-CoV-2 receptor ACE2 and TMPRSS2 are primarily expressed in bronchial transient secretory cells. The EMBO journal 39 (10), e105114.
McAuley, J.L., Corcilius, L., Tan, H.-X., Payne, R.J., McGuckin, M.A., Brown, L.E., 2017. The cell surface mucin MUC1 limits the severity of influenza A virus infection. Mucosal Immunol 10, 1581–1593.
Menachery, VD, Dinnon, KH, III, Yount, BL, Jr, McAnarney ET, Gralinski, LE, Hale, A, Graham, RL, Scobey, T, Anthony, SJ, Wang, L, Graham, B, Randell, SH, Lipkin, WI, Baric, RS, 2020. Trypsin treatment unlocks barrier for zoonotic bat coronavirus infection. J Virol 94 e01774-19.
Milewska, A, Zarebski, M, Nowak, P, Stozek, K, Potempa, J, Pyrc, K, 2014. Human Coronavirus NL63 utilizes heparan sulfate proteoglycans for attachment to target cells. Journal of Virology 88, 13221–13230.
Mycroft-West, C., Su, D., Stefano Elli, S., Guimond, S., Miller, G., Turnbull, J., Yates, E., Guerrini, M., Fernig, D., Lima, M. and Skidmore, M. (2020) The 2019 coronavirus (SARS-CoV-2) surface protein (Spike) S1 Receptor Binding Domain undergoes conformational change upon heparin binding.
Neuman, B.W., Kiss, G., Kunding, A.H., Bhella, D., Baksh, M.F., Connelly, S., Droese, B., Klaus, J.P., Makino, S., Sawicki, S.G., Siddell, S.G., Stamou, D.G., Wilson, I.A., Kuhn, P., Buchmeier, M.J., 2011. A structural analysis of M protein in coronavirus assembly and morphology. Journal of Structural Biology 174, 11–22.
Oh, M.D., Park, W.B., Choe, P.G., et al., 2016. Viral Load Kinetics of MERS Coronavirus Infection. N Engl J Med 375, 1303–1305.
Pan, Y., Zhang, D., Yang, P., Poon, L.L.M., Wang, Q., 2020. Viral load of SARS-CoV-2 in clinical samples. The Lancet. 20, 411–412.
Peng, G., Sun, D., Rajashankar, K.R., Qian, Z., Holmes, K.V., Lia, F., 2012. Crystal structure of mouse coronavirus receptor binding domain complexed with its murine receptor. Proc. Natl. Acad. Sci. U.S.A. 108, 10696–10701.
Plante, J.A., Plante, K.S., Gralinski, L.E., Beall, A., Ferris, M.T., Bottomly, D., Green, R., McWeeney, S.K., Heise, M.T., Baric, R.S. and Menachery, V.D. (2020). Mucin 4 protects female mice from coronavirus pathogenesis. (10.1101/2020.02.19.957118).
Pulkkinen, L.I.A., Butcher, S.J., Anastasina, M., 2018. Tick-borne encephalitis virus: A structural view. Viruses 10, 350.
Ridley, C., Thornton, D.J., 2018. Mucins: the frontline defence of the lung. Biochemical Society Transactions (2018) 46, 1099–1106.
Santiana, M., Ghosh, S., Ho, B.A., Rajasekaran, V., Du, W.L., Mutsafi, Y., De Jésus-Diaz, D.A., Sosnovtsev, S.V., Levenson, E.A., Parra, G.I., Takvorian, P.M., Cali, A., Bleck, C., Vlasova, A.N., Saif, L.J., Patton, J.T., Lopalco, P., Corcelli, A., Green, K.Y., Altan-Bonnet, N., 2018. Vesicle-cloaked virus clusters are optimal units for inter-organismal viral transmission. Cell host & microbe 24 (2), 208–220.
Shang, J., Wan, Y., Liu, C., Yount, B., Gully, K., Yang, Y., Auerbach, A., Peng, G., Baric, R., Li, F., 2020. Structure of mouse coronavirus spike protein complexed with receptor reveals mechanism for viral entry. PloS Pathog 16 (3), e1008392.
Stonebraker, J.R., Wagner, D., Lefensty, R.W., Burns, K., Gendler, S.J., Bergelson, J.M., et al., 2004. Glycocalyx restricts adenoviral vector access to apical receptors expressed on respiratory epithelium in vitro and in vivo: role for tethered mucins as barriers to lumenal infection. J. Virol. 78, 13755–13768.
Taylor, M.E., Drickamer, K., 2006. Carbohydrate recognition in cell adhesion and signalling. In: Taylor, M.E., Drickamer, K. (Eds.), Introduction to glycobiology. Oxford University Press, Oxford, pp. 122–154.
To, K.K.-W., Tsang, O.T.-Y., Leung, W.-S., Tam, A.R., Wu, T.-C., Lung, D.C., Yip, C.C.-Y., Cai, J.-P., Chan, J.M.-C., Chik, T.S.-H., Lau, D.P.-L., Choi, C.Y.-C., Chen, L.-L., Chan, W.-M., Chan, K.-H., Ip, J.D., Ng, A.C.-K., Poon, R.W.-S., Luo, C.-T., Cheng, V.C.-C., Chan, J.F.-W., Hung, I.F.-N., Chen, Z., Chen, H., Yuen, K.-Y., 2020. Temporal profiles of viral load in posterior oropharyngeal saliva samples and serum antibody responses during infection by SARS-CoV-2: an observational cohort study. Lancet Infect. Dis. 20, 565–574.
Van Leuken, J.G.P., Swart, A.N., Havelaar, A.H., Van Pul, A., Van der Hoek, W., Heederik, D., 2016. Atmospheric dispersion modelling of bioaerosols that are pathogenic to humans and livestock – A review to inform risk assessment studies. Microbial Risk Analysis 1, 19–39.
Vicenzi, E., Canducci, F., Pinna, D., Mancini, N., Carletti, S., Lazzarin, A., Bordignon, C., Poli, G., Clementi, M., 2004. Coronaviridae and SARS-associated coronavirus strain HSR1. Emerging infectious diseases 10, 413–418.
Vogt, V.M., Simon, M.N., 1999. Mass determination of Rous sarcoma virus virions by scanning transmission electron microscopy. J Virol 73, 7050–7055.
Walls, A.C., Tortorici, M.A., Snijder, J., Xiong, X., Bosch, B.J., Rey, F.A., Veesler, D., 2017. Tectonic conformational changes of a coronavirus spike glycoprotein promote membrane fusion. PNAS 114, 11157–11162.
Walls, A.C., Park, Y.-J., Tortorici, M.A., Wall, A., McGuire, A.T., Veesler, D., 2020. Structure, function, and antigenicity of the SARSCoV-2 spike glycoprotein. Cell 180, 281–292.
Watanabe, T., Bartrand, T.A., Weir, M.N., Omura, T., Haas, C.N., 2010. Development of a dose-response model for SARS coronavirus. Risk Analysis 30, 1129–1138.
Weir, M.H., Haas, C.N., 2011. A model for in-vivo delivered dose estimation for inhaled Bacillus anthracis spores in humans with interspecies extrapolation. Environmental Science and Technology 45, 5828–5833.
Wrapp, D., Wang, N., Corbett, K.S., et al., 2020. Cryo-EM structure of the 2019-nCoV spike in the prefusion conformation. Science 367, 1260–1263.
Yang, X., Kurteva, S., Ren, X., Lee, S., Sodroski, J., 2005. Stoichiometry of envelope glycoprotein trimers in the entry of human immunodeficiency virus type 1. J. Virol. 79, 12132–12147.
Yuan, Y., Cao, D., Zhang, Y., Ma, J., Qi, J., Wang, Q., Lu, G., Wu, Y., Yan, J., Shi, Y., Zhang, X., Gao, G.F., 2017. Cryo-EM structures of MERS-CoV and SARS-CoV spike glycoproteins reveal the dynamic receptor binding domains. Nature Communications 8, 15092.
Zanin, M., Baviskar, P., Robert Webster, R, Richard Webby, R, 2016. The interaction between respiratory pathogens and mucus. Cell Host & Microbe 19, 159–168.
Zhang, L., Lin, D., Sun1, X., Curth, U., Drosten, X., Sauerhering, L., Becker, S., Rox, K., Hilgenfeld, R., 2020. Crystal structure of SARS-CoV-2 main protease provides a basis for design of improved α-ketoamide inhibitors. Science. https://doi.org/10.1126/science.abb3405.